NASA TN D-1021

TECHNICAL NOTE

D-1021

ANALYTICAL AND EXPERIMENTAL INVESTIGATION OF FLUTTER AND DIVERGENCE OF SPRING-MOUNTED CONE CONFIGURATIONS AT SUPERSONIC SPEEDS

By John L. Sewall, Robert W. Hess, and
Charles E. Watkins

Langley Research Center
Langley Station, Hampton, Va.

NATIONAL AERONAUTICS AND SPACE ADMINISTRATION

WASHINGTON April 1962

1G

NATIONAL AERONAUTICS AND SPACE ADMINISTRATION

TECHNICAL NOTE D-1021

ANALYTICAL AND EXPERIMENTAL INVESTIGATION OF FLUTTER AND DIVERGENCE OF SPRING-MOUNTED CONE CONFIGURATIONS AT SUPERSONIC SPEEDS

By John L. Sewall, Robert W. Hess, and
Charles E. Watkins

SUMMARY

This paper reports the results of an analytical and experimental study of flutter and static divergence of a rigid conical shell mounted on springs that permitted freedom in vertical translation and pitch. The test program was conducted with air as the test medium in the Langley 9- by 18-inch supersonic aeroelasticity tunnel at Mach numbers 1.64, 2, and 3 and with helium in the Langley 8-inch hypersonic aeroelasticity tunnel at a Mach number of 6.83 and in the Langley 24-inch hypersonic aeroelasticity tunnel at a Mach number of 15.4. Flutter calculations were made based on several slender-body theories for approximating the oscillating aerodynamic forces and moments acting on the cone. Good agreement with experimental results was obtained for the quasi-steady aerodynamic approaches of Van Dyke and Von Karman at low supersonic speeds and for Newtonian theory at hypersonic speeds. Pitch-axis position and translation-to-pitch frequency ratio had a pronounced effect on the flutter speed boundary, particularly near a frequency ratio of 1. No flutter was encountered experimentally or predicted analytically when the center of gravity of the model was ahead of the pitch axis.

With the model restrained to permit only the pitch degree of freedom, static divergence was obtained at the low supersonic Mach numbers for the pitch axis at three-fourths of the cone length measured from the nose of the cone, but the agreement of experimental with calculated divergence conditions was poor and showed no consistent trend with respect to variation in Mach number. The introduction of an axial force, based on steady total drag measurements, into the flutter calculations resulted in higher theoretical flutter speed boundaries for frequency ratios less than 1 and slightly lower flutter speed boundaries for frequency ratios greater than 1. For some calculations the direction of the axial force was arbitrarily reversed, and this change resulted in lower flutter speed boundaries for frequency ratios less than 1 and slightly higher boundaries at frequency ratios greater than 1. The effect of a steady drag force on theoretical divergence boundaries was to raise the divergence speed parameter above that for zero drag for pitch axes at which divergence occurs and to lower it for an oppositely directed steady axial force.

INTRODUCTION

Although much of the effort spent in the development of the theory for aerodynamic forces on slender bodies has dealt with steady-state conditions, a considerable part of the theory already developed can be extended to apply to unsteady conditions. Such extensions yield what are commonly called quasi-steady aerodynamics. To go beyond the quasi-steady concept, one must deal with the velocity potential for unsteady motion, but the extent to which this can be satisfactorily done is severely limited. In fact, all known approaches for determining body forces are subject to more or less stringent limitations. For example, in the quasi-steady concept, the frequency of oscillation must be small and, in general, the similarity parameter $\sqrt{|M^2 - 1|}\,\tau \ll 1$ for supersonic flow and $M\tau > 1$ for hypersonic flow (M being the Mach number and τ the body thickness ratio or some local slope such as the nose angle). The second of these limitations, which holds for steady as well as unsteady flow, implies that none of theoretical methods to date can be relied on throughout the subsonic and supersonic speed ranges, particularly in the transonic region or in a range where $\sqrt{|M^2 - 1|}\,\tau$ is neither large nor small.

This paper reports an investigation aimed at making some evaluations of existing theories that can be applied to unsteady conditions. This effort mainly involved the calculation of the flutter boundaries of simple spring-mounted cones and comparison of the results with experimental results at supersonic Mach numbers ranging from 1.64 to 15.4. The cones were actually light hollow shells which were, for all practical purposes, rigid, flexibility being provided by springs that permitted vertical translation of and pitch about an axis that could be fixed at various positions along the axis of the cone. This simplified configuration was chosen because its structural characteristics could be accurately represented. Thus, any differences between theory and experiment would be due mainly to the aerodynamic representation in the theory.

The aerodynamic theories considered in this study are the Munk-Jones or momentum theory (ref. 1), the frequency expansion of the velocity potential of first-order slender-body theory (refs. 2 and 3), Von Karman's approximation for a cone (ref. 4), Van Dyke's second-order theory (ref. 5), a piston-theory approximation of Miles and Young (ref. 6), shock expansion theory (ref. 7) treated in the sense suggested by Eggers and Savin (ref. 8), and Newtonian theory with two modifications (refs. 9 to 11).

Although the present paper is primarily concerned with flutter, the static aeroelastic phenomenon of divergence is also considered, and some

limited comparisons with experiment are made. Provision is also made in the basic flutter and divergence analysis for the introduction of a steady axial force. Results of some calculations are presented including such a force in the form of a steady-state drag coefficient, and values of this coefficient are based on measured base pressures and drag forces on the models used for the flutter and divergence tests.

SYMBOLS

a	free-stream speed of sound
A_{hh}	aerodynamic coefficient in pure translation in flutter equation (eq. (2))
$A_{h\alpha}, A_{\alpha h}$	aerodynamic translation-pitch coupling coefficients in flutter equation
$A_{\alpha\alpha}$	aerodynamic coefficient in pure pitch in flutter equation
b	length of cone measured along axis of cone
C_p	pressure coefficient
C_D	total drag coefficient
C_{mD}	moment coefficient due to drag, $C_{mD} = C_D\bar{x}_D$
D	drag force, positive aft, $q\pi b^2 C_D$, lb
f	frequency, $\omega/2\pi$
F	function proportional to pressure coefficient as derived for quasi-steady theories (see table following eq. (7a))
$f(t)$, $f(t_0)$	harmonic functions of time in shock expansion theory (see appendix)
g	structural damping coefficient in eigenvalue for flutter (see eq. (2))
h_0	translational amplitude of pitch axis of cone flutter model, positive down
I_α	mass moment of inertia of cone flutter model in pitch about pitch axis

f_α	uncoupled pitching frequency
f_f	flutter frequency
f_n	nth natural (coupled) frequency where $n = 1,2$
K_c	term by which downwash is introduced into Von Karman's quasi-steady theory (see appendix)
$k = \frac{\frac{b}{2}\omega}{V}$	reduced frequency
k_α	spring constant of cone flutter or divergence model in pitch
$l(x)$	lift per unit length acting on cone, lb/ft
L	generalized lift (see eq. (3))
L_1, L_3	lift components of real aerodynamic coefficients in frequency-expansion method
L_2, L_4	imaginary lift components of aerodynamic coefficients in frequency-expansion method
m	mass of cone flutter model free to pitch
m_h	mass of cone flutter model in vertical translation
M	free-stream Mach number
M_α	generalized aerodynamic moment about pitch axis (see eq. (4))
M_1, M_3	real moment components of aerodynamic coefficients in frequency-expansion method
M_2, M_4	imaginary moment components of aerodynamic coefficients in frequency-expansion method
$\bar{M}_N$	Mach number of unyawed cone at its apex behind shock wave on surface of cone
M_S	Mach number immediately behind shock wave at nose of cone
n	index

p	pressure on body surface
$\bar{p}_N$	pressure on unyawed cone at its apex behind shock wave on surface of cone
p_∞	free-stream static pressure
q	dynamic pressure
q_d	dynamic pressure at divergence
Q	function of $M\delta$ and γ given by equation (A16)
$r(x)$	radius of body of revolution at distance x from the nose, $r_b\bar{r}$
r_b	base radius of body
r_α	dimensionless radius of gyration about pitch axis, $\sqrt{\frac{I_\alpha}{mb^2}}$
t	time
v	local normal velocity at point on surface of body of revolution
V	free-stream velocity
w	downwash velocity
x	distance along body center line and tunnel center line measured from nose of body, positive aft (see fig. 1), $b\bar{x}$
x_D	distance from pitch axis to center of drag force, $b\bar{x}_D$
x_α	distance from nose of body to pitch axis of cone flutter or divergence model, $b\bar{x}_\alpha$
x_g	distance from pitch axis to center of gravity of model in pitch, positive for center of gravity aft of pitch axis, $b\bar{x}_g$
$z(x,t)$	amplitude function specifying motion of body, see eq. (8a)

α_0 rotational amplitude of cone flutter model in pitch about pitch axis, positive nose up

$\beta = \sqrt{M^2 - 1}$

$\bar{\beta}$ angle between shock wave and body surface (see sketch following eq. (A13))

η parameter in shock-expansion theory given by eq. (A15)

δ semi-vertex angle of cone

$\Delta(x)$ series in lift expression for frequency expansion method (see eq. (5) and ref. 3)

γ ratio of specific heats

ω angular frequency, $2\pi f$

ω_h uncoupled angular frequency in vertical translation

ω_α uncoupled angular pitching frequency

ω_n nth natural (coupled) frequency where $n = 1,2$

Ω complex eigenvalue for flutter (see eq. (2)), $\left(\frac{\omega_\alpha}{\omega}\right)^2 (1 + ig)$

μ mass-density ratio, $\frac{m}{\pi\rho b r_b^2}$

ρ airstream density

$\mu_h = \frac{m_h}{m}\mu$

θ angular polar variable of integration around body of revolution (see sketch following eq. (6))

Nondimensional lengths are denoted by barred symbols unless otherwise specified.

EXPERIMENTAL PROGRAM

The experimental data used to provide a basis for evaluating various theories for calculating the oscillating aerodynamic forces on cones was obtained by testing simple spring-mounted cones in supersonic flow for flutter. These models and the necessary supporting apparatus were designed to permit translation of and pitch about an axis perpendicular to and intersecting the longitudinal axis of the cone. In addition to the flutter experiments, divergence tests were made at all Mach numbers except $M = 6.83$ and 15.4. Also, base pressures were measured at the lower Mach numbers, and total axial-force measurements were made at $M = 6.83$.

Properties of Models

The models consisted of hollow conical shells mounted on springs as shown in figure 1. These conical shells were made from balsa wood laminated with paraplex and fiber glass and were reinforced at the trailing edge with a fiber glass ring mounted just inside the cone. This construction resulted in a shell structure that was for all practical purposes rigid with respect to the mounting springs. Flexibility of the model in pitch was provided by a flex hinge which, as shown in figure 1(a), is composed of a pair of Swedish steel straps crossed between two steel blocks. The pitch axis was located at the intersection of the straps and variations in the hinge stiffness were obtained by varying the strap thickness. Flexibility in translation was obtained from the arrangement of two parallel straps shown on figure 1(a). This arrangement permitted only vertical translation of the pitch axis. The translation stiffness was varied by varying the length of the straps for a particular strap thickness.

The mass of the model free to pitch m consisted of the mass of the cone and its aluminum mounting bar plus the mass of the pitching springs and the forward mount block. The mass of the model in translation m_h consisted of the mass of the model in pitch plus the mass of the aft mounting block and the effective mass of the translation springs. The effective mass of the translation springs was estimated to be 0.37 times the actual mass of the springs. Geometric and inertial properties of the models are listed in table I.

In order to keep the structural damping as low as possible and to minimize the structural differences between models, the springs were clamped to the steel blocks as tightly as possible.

Test Program

The experimental program was conducted in the Langley 9- by 18-inch supersonic aeroelasticity tunnel at Mach numbers 1.64, 2, and 3 and in the Langley 8-inch hypersonic aeroelasticity tunnel at a Mach number of 6.83. In addition, one flutter test point was obtained in the Langley 24-inch hypersonic aeroelasticity tunnel at a Mach number of 15.4. For each model at each Mach number, the stiffnesses were varied, as previously noted, to obtain a wide range of uncoupled translation-to-pitch frequency ratios. This parameter was obtained from the relation

$$\frac{\omega_h}{\omega_\alpha} = \sqrt{\frac{1}{\left(\frac{\omega_\alpha}{\omega_1}\right)^2 + \left(\frac{\omega_\alpha}{\omega_2}\right)^2 - 1}} \qquad (1)$$

in terms of the measured natural (coupled) frequencies ω_1, ω_2, and the measured uncoupled pitching frequency ω_α. These frequencies were obtained by shaking the model with an air jet shaker (similar to that described in ref. 12) prior to each tunnel run and by reading oscillograph traces of signals from resistance-wire strain gages mounted on both translation and flex hinge straps. The uncoupled pitching frequency was obtained with a spacer wedged between the translation spring straps to eliminate the translational degree of freedom. Damping coefficients were measured from records of the decay of free oscillations and were found to be very small (that is, $g \approx 0.005$ to 0.01).

In the operation of the tunnels, the Mach number was held constant whereas the test-section density was increased until flutter occurred. A recording oscillograph was used to obtain a continuous record of tunnel stagnation temperature and pressure. Strain-gage signals on the same oscillograph record were used to indicate the onset of flutter and to determine the flutter frequency. Divergence conditions were determined for model 4 ($\bar{x}_\alpha = 0.75$) for Mach numbers 1.64, 2, and 3, the translational freedom being eliminated by substitution of a solid bar for the translation springs. The onset of divergence was determined from the flex-hinge strain-gage signals.

Axial-Load Measurements

The total steady aerodynamic drag acting on the cone mounted on the sting was estimated for three of the Mach numbers tested by a combination of measured and calculated data. At $M = 2$ and $M = 3$ the total drag coefficient C_D was approximated from measured base-pressure data

together with calculated forebody pressure drag and skin-friction drag coefficients. At $M = 6.83$, C_D was obtained from force measurements made on a model fitted with an axial-load cell rigidly attached to the sting. Values of C_D are listed in table II. The two different values for each Mach number result from the variation of C_D with Reynolds number corresponding to the wide ranges of dynamic pressures covered in the test programs.

Experimental Results

The experimental flutter and divergence data are listed in table III. Flutter was obtained at four of the Mach numbers over a wide range of frequency ratios for all models except those in which the center of gravity was ahead of the pitch axis ($\bar{x}_g$ negative in table I).

The flutter results in table III are shown in coefficient form as functions of frequency ratio in figures 2 to 11. The flutter speed is given in the upper parts of the figures in terms of a stiffness-altitude parameter similar to that so widely used in wing flutter. For the test ranges of mass-density ratio $1/\mu$ and pitch frequency ω_α, all the flutter speed data for a given pitch-axis position tend to lie on the same curve. The flutter frequency is given in the lower parts of figures 2 to 11 in terms of the ratio ω_α/ω_f which also appeared to be unaffected by changes in density or pitch stiffness.

Note that the experimental flutter speed appeared to be highly sensitive to frequency ratios very close to 1. This is particularly evident in figures 2, 3, and 5 to 8 where the flutter speed dropped to a low point between $\frac{\omega_h}{\omega_\alpha} = 1.0$ to $\frac{\omega_h}{\omega_\alpha} = 1.2$ from a no-flutter condition at $\frac{\omega_h}{\omega_\alpha} \approx 1.0$. It is also evident that this minimum point tends to decrease slightly with increasing Mach number from $M = 1.64$ to $M = 3$ but experiences more of a reduction at $\bar{x}_\alpha = 0.58$ than at $\bar{x}_\alpha = 0.5$. The effect of pitch axis, including $\bar{x}_\alpha = 0.667$, is also mentioned later in connection with the analytical flutter boundaries.

The divergence tests on model 4 at Mach numbers 1.64, 2, and 3 resulted in near linear variations of dynamic pressure with f_α^2 (proportional to pitch stiffness) as shown in figure 12. The scatter in the data at Mach number 2 may be due to the fact that more difficulty was encountered here than at the other two Mach numbers in detecting the

onset of divergence. The slope of each trend in figure 12 is proportional to the divergence parameter $\frac{2\pi q_d b r_b^2}{\omega_\alpha^2 I_\alpha}$ $\left(\text{or } \frac{2\pi q_d b r_b^2}{k_\alpha}\right)$ which is shown as a function of Mach number in figure 13.

ANALYTICAL STUDIES AND COMPARISON WITH EXPERIMENT

The analytical work of this investigation is reported and compared with experiment in this section. This work consisted mainly of calculating flutter boundaries for the spring-mounted cones by using various slender-body theories to approximate the oscillating aerodynamic forces and moments acting on the cone. The basic flutter equation is presented for the translation and pitching degrees of freedom shown schematically in figure 1(b). Included also in this section is the equation for static divergence. Provision is made in the aerodynamic forces for the addition of a steady total axial force in both flutter and divergence equations, and calculations to determine the effect of this force are based on measured drag data.

Flutter Equation

The flutter equation, derived in the usual manner for the system shown in figure 1(b) is, in matrix form, as follows:

$$\begin{bmatrix} 1 - \left(\frac{\omega_h}{\omega_\alpha}\right)^2 \Omega + \frac{A_{hh}}{\mu_h} & \frac{m}{m_h}\bar{x}_g + \frac{A_{h\alpha}}{\mu_h} \\ \bar{x}_g + \frac{A_{\alpha h}}{\mu} & (1 - \Omega) r_\alpha^2 + \frac{A_{\alpha\alpha}}{\mu} \end{bmatrix} \begin{Bmatrix} \frac{h_0}{b} \\ \alpha_0 \end{Bmatrix} = \begin{Bmatrix} 0 \\ 0 \end{Bmatrix} \tag{2}$$

The aerodynamic coefficients A_{hh}, $A_{h\alpha}$, $A_{\alpha h}$, and $A_{\alpha\alpha}$ are obtained from the generalized lift and moment expressions

$$L = \int_0^b l(x)\, dx = \pi\rho b^2 r_b^2 \omega^2 \left(A_{hh}\frac{h_0}{b} + A_{h\alpha}\alpha_0\right) \tag{3}$$

and

$$M_\alpha = \int_0^b (x - x_\alpha) l(x)\, dx = \pi\rho b^3 r_b^2 \omega^2 \left(A_{\alpha h} \frac{h_0}{b} + A_{\alpha\alpha}\alpha_0 \right) \qquad (4)$$

In the following sections expressions for $l(x)$ are given for each of the slender-body theories considered in this study. Corresponding expressions for A_{hh}, $A_{h\alpha}$, and so forth, are listed in table IV.

L
1
2
6
2

Unsteady Aerodynamic Coefficients

A limiting form of the velocity potential for the oscillatory case is known in the form of definite integrals. (See, for example, ref. 2.) These integrals can be evaluated by expanding the integrands in powers of reduced frequency k as is done in references 2 and 3 or by numerical integration procedures such as those used in reference 13. In reference 3 the frequency expansion is carried to the fifth power of k for the motions considered in the present study, and the lift per unit length is given therein by the expression

$$l(x) = -\pi\beta\rho V r(x)\, \Delta(x) \qquad (5)$$

for an arbitrary body of radius $r(x)$, where $\beta = \sqrt{M^2 - 1}$ and $\Delta(x)$ is a series of terms that are functions of Mach number and mode shape for the cone. Use of this series in equation (5) is shown in reference 3 to give the aerodynamic coefficients listed in table IV. The L and M terms in these coefficients are functions of Mach number, mode shape, and reduced frequency and are also given in detail in reference 3. This method is valid for low values of $\bar{\omega} = \frac{2kM^2}{\beta^2}$ and was applied in the present study for Mach numbers of 1.64, 2, and 3.

Quasi-Steady Aerodynamic Coefficients

Applications involving closed-form solutions.- An extension of steady-flow theory to the unsteady case for a body of revolution basically involves the introduction of the downwash into an expanded form of the steady-state pressure coefficient. The lift per unit length is then obtained by circumferential integration of the vertical component of the pressure at a point on the body surface, that is, through the relation

$$l(x) = qr(x) \int_0^{2\pi} C_p \sin\theta \, d\theta \tag{6}$$

where q is the dynamic pressure, θ is the variable of integration as shown in the following sketch, and C_p is the pressure coefficient which is a function of Mach number, local slope of the body surface, and downwash and specifies the motion of the body. (Further details on the form of C_p used in eq. (6) are given in the appendix for two particular theories.)

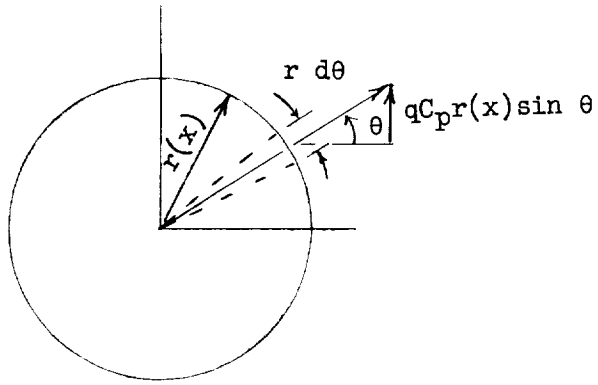

Performance of the indicated integration in equation (6) leads to

$$l(x) = -\pi\rho V r(x) F w \tag{7a}$$

For a cone of semi-vertex angle δ

$$l(x) = -\pi\rho V x \delta^2 (F/\delta) w \tag{7b}$$

where the quantity F/δ is given in the following table for the quasi-steady theories considered in this paper. (The introduction of the negative sign in eqs. (7) makes the direction of pressure indicated in the foregoing sketch compatible with the direction for positive downwash components h and α indicated in fig. 1(b).)

THEORY	F/δ
Munk-Jones (ref. 1)	$2 + \frac{x}{V}\left(V\frac{\partial}{\partial x} + \frac{\partial}{\partial t}\right)$
Von Karman (ref. 4)	$2\left(\log\frac{2}{\beta\delta} - 1\right)$
Van Dyke's 2d order theory (ref. 5)	$2\left[1 - \delta^2\left(M^2\log\frac{2}{\beta\delta} - \frac{3}{2}M^2 + 1\right)\right]$
Piston theory (ref. 6)	$\frac{1}{M\delta} + \frac{\gamma+1}{2} + \frac{\gamma+1}{4}M\delta$
Newtonian theory (refs. 9 to 11)	$\frac{F}{\delta} = 2$, (ref. 9) $\frac{F}{\delta} = \gamma + 1$, (ref. 10) $\frac{F}{\delta} = C_{p_{max}} \approx \frac{\gamma+3}{\gamma+1}\left(1 - \frac{\gamma+2}{\gamma+3}\frac{1}{M}\right)$, (ref. 11)

The ratio of specific heats is denoted by γ.

The first of these theories, also known as the momentum theory, is seen to be independent of Mach number. The next two theories apply to low supersonic Mach numbers and the last two to high supersonic Mach numbers.

The downwash w in equations (7) is given by

$$w = V\frac{\partial z}{\partial x} + \frac{\partial z}{\partial t} \tag{8a}$$

where z specifies the motion of the body and in the present study is given by

$$z(x,t) = \bar{z}(x)f(t) = \bar{z}(x)e^{i\omega t} \tag{8b}$$

with

$$\bar{z}(x) = h_0 + (x - x_\alpha)\alpha_0 \tag{8c}$$

for the oscillatory translation and pitch degrees of freedom represented in figure 1(b). The lift per unit length is thus completely determined, and use of equation (7a) with equations (8) in equations (3) and (4) leads to the quasi-steady aerodynamic coefficients listed in table IV.

Application of shock-expansion theory.- This method also involves a quasi-steady approach with the lift per unit length given by equation (6) and the pressure coefficient by the basic expression

$$C_p = \frac{2}{\gamma M^2}\left(\frac{p}{p_\infty} - 1\right) \tag{9}$$

where p is the pressure on the surface of the body and p_∞ is the pressure in the undisturbed stream ahead of the body. The pressure ratio p/p_∞ is derived in reference 7 for high supersonic speeds in terms of the downwash and the approximate expressions of reference 8 for pressure ratio and Mach number on the surface of the body behind the shock wave at the nose. These approximations of reference 8 are in turn functions of the shock-wave inclination corresponding to the slope of the body at the nose.

The application of this method to the $7\frac{1}{2}^\circ$ (semi-vertex angle) cone of the present study is demonstrated in the appendix for Mach number 6.83, and the specific lift per unit length for this case is shown to be

$$l(x) = -\frac{3.86q\pi x\delta}{M}\left[\frac{i\omega h_0}{V} + \alpha_0 + \frac{i\omega}{V}(1.572x - x_\alpha)\alpha_0\right] \tag{10}$$

The introduction of this equation into the flutter equation (eq. (2)) by means of equations (3) and (4) results in the aerodynamic coefficients also listed with those of other theories in table IV.

Divergence Equations

With $h_0 = 0$ and $\omega = 0$ in equation (2), the equation for static divergence is given by

$$k_\alpha\alpha_0 = \omega_\alpha^2 I_\alpha\alpha_0 = M_\alpha \tag{11}$$

where M_α is based solely on the steady-state part of the aerodynamic forces and k_α is the spring constant of the model in pitch. For the Munk-Jones theory, equation (11) reduces to

$$\frac{2\pi q_d b r_b^2}{k_\alpha} = -\frac{1}{1 - \bar{x}_\alpha - \int_0^1 \bar{r}^2 d\bar{x}} \tag{12}$$

$$\frac{2\pi q_d b r_b^2}{k_\alpha} = -\frac{1}{\frac{2}{3} - \bar{x}_\alpha} \tag{12a}$$

for the cone, where q_d is the dynamic pressure at divergence. Equation (12a) is plotted in figure 14 as a function of pitch-axis position, and, as may be seen, the cone is free from divergence for pitch axes located in the first two-thirds of its length.

From equation (11), it can be shown that the divergence equation based on the frequency expansion theory (ref. 3) is given by

$$\frac{2\pi q_d b r_b^2}{k_\alpha} = \frac{-1}{\left(\frac{2}{3} - \bar{x}_\alpha\right)\sqrt{1 - (\beta \tan \delta)^2}} \tag{13}$$

Similarly, for the quasi-steady theories of Von Karman, Van Dyke, and Newton, together with piston theory due to Miles and Young, equation (11) reduces to

$$\frac{2\pi q_d b r_b^2}{k_\alpha} = -\frac{1}{\frac{F}{\delta}\left(\frac{1}{3} - \frac{\bar{x}_\alpha}{2}\right)} \tag{14}$$

Note that for the Newtonian theory for $\frac{F}{\delta} = 2$, equation (14) becomes identical to equation (12a) which is based on the Munk-Jones theory.

Equations (13) and (14) are also plotted in figure 14, equation (14) being for both the Von Karman and Van Dyke theories. The frequency expansion and Van Dyke theories are shown for a Mach number of 3 and, as indicated by the close agreement with the Munk-Jones theory, predict a small Mach number effect. This is seen more clearly in figure 13

where, in contrast, the Von Karman and piston theories predict a substantial Mach number effect.

Analytical Results and Comparison With Experiment

Results of flutter and divergence calculations based on the aerodynamic theories described in the preceding sections are presented and compared with experimental results in figures 2 to 11 for flutter and in figure 13 for divergence. The effect of introducing a steady total axial force into the analysis in terms of drag coefficient is discussed herein and shown in figures 15 to 20 for flutter and in figure 21 for divergence.

Flutter.- From the analytical flutter speed boundaries in the upper parts of figures 2 to 11, it is evident that the different aerodynamic theories used in the flutter analysis generally tend to be more distinguishable from one another for frequency ratios greater than 1 than for frequency ratios less than 1. As the pitch axis was moved aft, this distinction lessened, and the minimum points in the different boundaries were lowered. The effect of pitch-axis position is particularly evident for the case of $M = 6.38$ when $\bar{x}_\alpha = \frac{2}{3}$. The Munk-Jones theory gives the lowest value of $\frac{V}{\frac{b}{2}\omega_\alpha\sqrt{\mu}}$ in all cases considered, and this minimum value, although it appears to be, is not zero. The frequency ratio at which this minimum occurred decreased as the pitch axis was moved aft (compare, for example, figs. 2 and 3) but, as the center of gravity was moved aft for a given pitch axis, the frequency ratio for this minimum point increased. (See fig. 5.)

Comparisons of analytical with experimental flutter speed boundaries show the Van Dyke and Newtonian theories to be in better agreement with experiment than the other theories, although this is less evident at $M = 6.83$ (for the Newtonian theory), because of the fewer number of experimental points obtained at this Mach number.

In contrast to the behavior noted for $\frac{V}{\frac{b}{2}\omega_\alpha\sqrt{\mu}}$, the parameter ω_α/ω_f showed consistently smooth variations throughout the entire range of frequency ratios covered. Moreover, regardless of the aerodynamic theory used, the flutter frequency appears to follow the same general trend, and all the theories considered give good agreement with experiment.

Divergence.- Comparison between theoretical and experimental divergence trends in figure 13 shows poorer and less consistent agreement than that obtained for flutter. No definite explanation is offered for the apparent Mach number effect indicated by the Von Karman and piston theories in contrast to the trends of the other theories. As may be seen in figure 14, this large effect is not confined to $\bar{x}_\alpha = \frac{3}{4}$ but is magnified at this location probably because of its proximity to the infinite discontinuity at $\bar{x}_\alpha = \frac{2}{3}$ (which is also the center of pressure of the cone).

Consideration of axial force.- Whereas axial forces have seldom been considered in aeroelastic problems on lifting surfaces, the greatly increased aerodynamic drag due to the blunter aerodynamic shapes of missile configurations together with the large deceleration forces experienced by these configurations have drawn attention to the possible effects of axial forces on the aeroelastic behavior of bodies of revolution, which, of course, form the basic shapes of missiles. In the present flutter and divergence studies of cones with their apexes pointed upstream, a steady axial force D is included with the other forces in the analysis and is assumed to be acting at a distance x_D aft of the pitch axis as shown in figure 1(b). The presence of this force gives rise to a moment about the pitch axis and tends to decrease the angle of attack so that the generalized moment given by equation (4) becomes

$$M_\alpha = \int_0^b (x - x_\alpha) l(x)\, dx - D(x_D\alpha) \tag{15}$$

$$M_\alpha = \int_0^b (x - x_\alpha) l(x)\, dx - C_D q \pi b^2 x_D \alpha \tag{15a}$$

where the axial force is written in terms of a drag coefficient C_D that is based on the total of all steady drag forces acting on the cone. This modification of the generalized moment in pitch results in the addition of the quantity $-\frac{1}{8k^2} C_{mD}$ to the coefficient $A_{\alpha\alpha}$ in the flutter equation (see table IV), C_{mD} being a moment coefficient due to drag given by $C_{mD} = C_D \bar{x}_D$. The divergence equations with the effect of drag included are

$$\frac{2\pi q_d b r_b^2}{k_\alpha} = -\frac{1}{1 - \bar{x}_\alpha - \int_0^1 \bar{r}^2 d\bar{x} + \frac{C_{mD}}{2}} \tag{16}$$

for the Munk-Jones theory,

$$\frac{2\pi q_d b r_b^2}{k_\alpha} = \frac{-1}{\left(\frac{2}{3} - \bar{x}_\alpha\right)\sqrt{1 - (\beta \tan \delta)^2} + \frac{C_{mD}}{2}} \tag{17}$$

for the frequency expansion method, and

$$\frac{2\pi q_d b r_b^2}{k_\alpha} = \frac{-1}{\frac{F}{\delta}\left(\frac{1}{3} - \frac{\bar{x}_\alpha}{2}\right) + \frac{C_{mD}}{2}} \tag{18}$$

for the quasi-steady theories.

The effect of introducing a steady total drag force into the flutter analysis in the manner just described is shown in figures 15 to 20 for the Van Dyke and Newtonian theories. Similar effects on the analytical flutter boundaries have been obtained for the Munk-Jones and Von Karman theories. The values of C_{mD} used in the calculations are based on the values of C_D given in table II. In figures 15 to 19 the effect of positive values of C_{mD} is to reduce the sizes of the flutter regions for $\bar{x}_\alpha = 0.5$ and $\bar{x}_\alpha = 0.58$, and for each pitch axis and Mach number there is a minimum frequency ratio below which the cone is flutter free. It may also be of interest to note in figures 15 to 19 that the left branches of the theoretical flutter boundaries with positive values of C_{mD} tend to lie somewhat closer to the experimental flutter points than do the theoretical flutter boundaries for $C_{mD} = 0$. However, for frequency ratios greater than 1, the agreement between theory and experiment is slightly better for $C_{mD} = 0$ than for $C_{mD} > 0$.

A few flutter calculations were performed with the sign of C_{mD} arbitrarily changed from plus to minus in order to determine the effect on flutter of an axial force in the flight direction, such as the force due to decelerated flight. The results of these calculations are shown in figures 19 and 20 for $C_{mD} = -0.03$ and -0.02, respectively, and the

effect is seen to be opposite to that found for $C_{mD} = 0.03$ and 0.02. That is, for $\bar{x}_\alpha = 0.5$ (fig. 19) the flutter region is enlarged, and for $\bar{x}_\alpha = 0.667$ (fig. 20) there is a maximum frequency ratio above which the cone is flutter free. The lower parts of figures 15 to 20 indicate that the flutter frequency is not appreciably affected by the introduction of a steady axial force.

Some effects of axial forces on the theoretical divergence characteristics are shown in figure 21 for the Munk-Jones and Newtonian $\left(\frac{F}{\delta} = 2\right)$ theories. For the range of values of C_{mD} used in the flutter calculations, the effect of positive values of C_{mD} is to increase the theoretical divergence speed above the divergence speed for $C_{mD} = 0$, and the effect of negative C_{mD} is to decrease divergence speed below that for $C_{mD} = 0$. At $\bar{x}_\alpha = \frac{3}{4}$, the agreement with experiment is worse for $C_{mD} > 0$ than for $C_{mD} = 0$.

L
1
2
6
2

CONCLUDING REMARKS

This paper reports the results of an experimental and analytical study of the flutter and divergence behavior of rigid conical shells spring mounted with freedom to translate vertically and pitch in supersonic flow. Translation-to-pitch frequency ratio was varied over a wide range above and below a frequency ratio of 1, and three pitch-axis positions were examined for flutter and one pitch-axis position for divergence. Results given in terms of a stiffness-altitude parameter similar to that used in wing flutter show a strong effect of pitch-axis position and frequency ratio on the flutter-speed boundaries, particularly near a frequency ratio of 1.

The distinction between several slender-body theories for approximating the oscillating aerodynamic forces and moments in the flutter calculations generally tends to be more evident at frequency ratios greater than 1 than at frequency ratios very close to 1. Comparison of analytical with experimental flutter-speed boundaries shows the quasi-steady theories, particularly Van Dyke's second-order theory, to be in better agreement with experiment than are the other theories at low supersonic Mach numbers. No flutter was encountered experimentally or predicted analytically when the center of gravity of the model was ahead of the pitch axis.

Agreement between calculated and experimental static divergence boundaries for a cone with pitch axis at three-fourths the length of the cone, measured from the nose, is poor and not consistent with respect to variation in Mach number. In other words, none of the theories used showed a consistent agreement - or even a lack of agreement - with experiment for the Mach numbers considered.

The introduction of an axial force based on steady total drag measurements into the flutter calculations resulted in increased theoretical flutter-speed boundaries for frequency ratios less than 1 and slightly decreased boundaries for frequency ratios greater than 1. For an arbitrary change in the direction of the axial force at a Mach number of 6.83, the reverse trends were obtained.

Langley Research Center,
National Aeronautics and Space Administration,
Langley Air Force Base, Va., December 4, 1961.

APPENDIX

ON THE USE OF THE STEADY-STATE PRESSURE COEFFICIENT IN DETERMINING QUASI-STEADY AERODYNAMIC COEFFICIENTS FOR BODIES OF REVOLUTION

L 1 2 6 2

As noted in the main body of this paper, the extension of steady-flow theory to the unsteady case for a body of revolution basically involves the introduction of the downwash into an expanded form of the steady-state pressure coefficient. Pertinent details of this procedure are presented briefly in this appendix for the Von Karman and shock expansion theories.

Von Karman Theory

In the method due to Von Karman (ref. 4), the steady-state pressure coefficient can be written as

$$C_p = \frac{2K_c^2}{M^2}\left(\log \frac{2M}{\beta K_c} - \frac{1}{2}\right) \tag{A1}$$

where

$$K_c = \frac{v}{a} = \frac{V}{a}\left[\frac{dr}{dx} + \frac{w(x,t)}{V}\sin\theta\right] \tag{A2a}$$

$$K_c = M\left(\delta + \frac{w}{V}\sin\theta\right) \tag{A2b}$$

for a cone of semi-vertex angle δ, v being the local normal velocity at a point on the surface of the body, and a the speed of sound in the undisturbed airstream. The derivation of equation (A2a) is based on the boundary condition requiring the vanishing of the velocity of flow normal to the body surface and involving the relation

$$v = V\frac{\partial r(x,t)}{\partial x} + \frac{\partial r(x,t)}{\partial t} \tag{A3}$$

where $r(x,t) = r(x) + z(x,t)\sin\theta$, as shown in reference 3, for example. Equation (A1) may be expanded in a Taylor's series about $w = 0$ to give (retaining only the first two terms of the series)

$$C_p \approx 2\delta^2\left(\log\frac{2}{\beta\delta} - \frac{1}{2}\right) + 4\delta\left(\log\frac{2}{\beta\delta} - 1\right)\frac{w}{V}\sin\theta \tag{A4}$$

Substitution of equation (A4) into equation (6) leads to

$$\left.\begin{aligned} l(x) &= 4qx\delta^2\left(\log\frac{2}{\beta b} - 1\right)\frac{w}{V}\int_0^{2\pi}\sin^2\theta\, d\theta \\ l(x) &= 4\pi qx\delta^2\left(\log\frac{2}{\beta\delta} - 1\right)\frac{w}{V} \end{aligned}\right\} \tag{A5}$$

for the lift per unit length. This equation may be put in the form of equation (7b).

Shock Expansion Theory

The pressure ratio used in equation (9) for the shock expansion theory at high supersonic Mach numbers is from reference 7 given by

$$\frac{p}{p_\infty} = \left(\frac{\bar{p}_N}{p_\infty}\right)\left\{1 + \gamma\bar{M}_N\sin\theta\left[\frac{d\bar{z}}{dx}f(t) + \bar{z}(x)\frac{1}{V}\frac{df(t)}{dt}\right]\right.$$
$$\left. + \sin\theta\left(\eta - \gamma\bar{M}_N\right)\left[\left(\frac{d\bar{z}}{dx}\right)_{x=0} f\left(t - \frac{x}{V}\right) + \frac{\bar{z}(0)}{V}\left.\frac{df(t_0)}{dt_0}\right|_{t-\frac{x}{V}}\right]\right\} \tag{A6}$$

for a cone, where $\bar{p}_N$ and $\bar{M}_N$ are the pressure and Mach number for the unyawed cone at its apex behind the shock wave on the surface of the cone, and where the motion of the body is specified by equation (8a). The

quantities $\frac{d\bar{z}}{dx}$ and $\bar{z}(0)$ are given by

$$\left.\begin{aligned} \frac{d\bar{z}}{dx} &= \alpha_0 \\ \bar{z}(0) &= h_0 - \alpha_0 x_\alpha \end{aligned}\right\} \tag{A7}$$

By letting $t = t_0 + \frac{x}{V}$

$$f\left(t_0\right) = e^{i\omega\left(t_0 + \frac{x}{V}\right)} \tag{A8}$$

and

$$\left.\frac{df(t_0)}{dt_0}\right|_{t-\frac{x}{V}} = i\omega e^{i\omega\left(t - \frac{x}{V}\right)} \tag{A9}$$

Substitution of equation (8a) and equations (A7) to (A9) into equation (A6) results in the following expression for the pressure ratio for a cone undergoing vertical translation of and pitch about an axis perpendicular to the axis of symmetry:

$$\frac{p}{p_\infty} = \left(\frac{\bar{p}_N}{p_\infty}\right)\left(1 + \gamma\bar{M}_N \sin\theta\left\{\alpha_0 + \frac{i\omega}{V}\left[h_0 + \alpha_0(x - x_\alpha)\right]\right\}\right.$$
$$\left. + \sin\theta\left(\eta - \gamma\bar{M}_N\right)\left[\alpha_0 + \frac{i\omega}{V}\left(h_0 - \alpha_0 x_\alpha\right)\right]e^{-\frac{i\omega}{V}x}\right)e^{i\omega t} \tag{A10}$$

The pressure ratio $\frac{\bar{p}_N}{p}$ and Mach number $\bar{M}_N$ are obtained from the following approximate expressions derived in reference 8:

$$\frac{\bar{p}_N}{p_\infty} = \left[1 + \gamma(M\delta)^2\right]\left(\frac{M_S}{\bar{M}_N}\right)^{\frac{2\gamma}{\gamma-1}} \tag{A11}$$

$$\left(\frac{\bar{M}_N}{M_S}\right)^2 = \left\{1 + \frac{\gamma - 1}{2}(M\delta)^2\left(\frac{M_S}{M}\right)^2\left[1 + \log\left(\frac{M\delta}{M\bar{\beta}}\right)^2 - \left(\frac{M\delta}{M\bar{\beta}}\right)^2\right]\right\} \tag{A12}$$

where

$$M\bar{\beta} = \sqrt{1 + \left(\frac{\gamma + 1}{2}\right)(M\delta)^2} \tag{A13}$$

and $\bar{\beta}$ is the angle between the shock wave and the cone surface as illustrated in the following sketch for the unyawed cone:

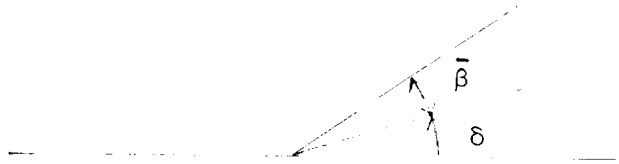

M_S is the Mach number immediately behind the shock wave at the nose of the cone, and

$$\left(\frac{M_S}{M}\right)^2 = \frac{1 + \frac{\gamma + 1}{2}(M\delta)^2}{\left[1 + \gamma(M\delta)^2\right]\left[\left(1 + \frac{\gamma - 1}{2}\right)(M\delta)^2\right]} \tag{A14}$$

The parameter η in equations (A6) and (A10) is obtained from the following relations given in reference 7:

$$\frac{\eta}{M} = \gamma Q\sqrt{1 + \frac{\gamma + 1}{2}(M\delta)^2}\left\{\left(\frac{\bar{M}_N}{M}\right)^2 - \frac{(M\delta)^4}{\left[1 + \frac{\gamma + 1}{2}(M\delta)^2\right]\left[1 + \frac{\gamma - 1}{2}(M\delta)^2\right]\left[1 + \gamma(M\delta)^2\right]}\right\} \tag{A15}$$

where

$$Q = \frac{1 + \dfrac{(M\delta)^2}{1 + \dfrac{\gamma + 1}{2}(M\delta)^2}}{\dfrac{\gamma + 5}{\gamma + 1} - \dfrac{M\delta}{\sqrt{1 + \dfrac{\gamma + 1}{2}(M\delta)^2}}} \tag{A16}$$

L
1
2
6
2

When the shock expansion theory was applied for $M = 6.83$, the following numerical values of the pertinent parameters given by equations (A10) to (A16) were used:

$\delta = 7.5^\circ$ ($\tan \delta = 0.1317$ actually used)

$M = 6.83$

$\gamma = \frac{5}{3}$ for helium

$M\bar{\beta} = 1.4418$

$\left(\frac{M_S}{M}\right)^2 = 0.82048$

$\left(\frac{\bar{M}_N}{M_S}\right)^2 = 0.92635$

$\frac{\bar{p}_N}{p_\infty} = 2.84355$

$\frac{\eta}{M} = 1.13125$

$Q = 0.74047$

By using these values in equation (A10) and substituting this equation into equation (9), the lift per unit length determined from equation (6) is

$$l(x) = -q\frac{2\pi x\delta}{M}\left(2.48\left\{\alpha_0 + \frac{i\omega}{V}\left[h_0 + \alpha_0(x - x_\alpha)\right]\right\}\right.$$
$$\left. - 0.5505\left[\alpha_0 + \frac{i\omega}{V}\left(h_0 - \alpha_0 x_\alpha\right)\right]e^{-\frac{i\omega}{V}x}\right)e^{i\omega t} \qquad \text{(A17)}$$

which reduces to equation (10) when $e^{-\frac{i\omega}{V}x}$ is approximated by $1 - \frac{i\omega}{V}x$, and $\left(\frac{i\omega}{V}\right)^2$ and higher power terms are neglected. The factor $e^{i\omega t}$ is, of course, eliminated by virtue of the assumption of simple harmonic motion initially in the derivation of the flutter equations.

REFERENCES

1. Miles, John W.: On Non-Steady Motion of Slender Bodies. Aero. Quarterly, vol. II, pt. III, Nov. 1950, pp. 183-194.

2. Dorrance, William H.: Nonsteady Supersonic Flow About Pointed Bodies of Revolution. Jour. Aero. Sci., vol. 18, no. 8, Aug. 1951, pp. 505-511, 542.

3. Lansing, Donald L.: Velocity Potential and Forces on Oscillating Slender Bodies of Revolution in Supersonic Flow Expanded to the Fifth Power of the Frequency. NASA TN D-1225, 1962.

4. Von Karman, Theodore: The Problem of Resistance in Compressible Fluids. R. Accad. d'Italia Cl. Sci. Fis., Mat. e. Nat., vol. XIV, 1936. (Fifth Volta Congress, Rome, Sept. 30-Oct. 6, 1935.)

5. Van Dyke, Milton D.: A Study of Second-Order Supersonic Flow Theory. NACA Rep. 1081, 1952. (Supersedes NACA TN 2200.)

6. Miles, J. W., and Young, Dana: Generalized Missile Dynamics Analysis. III - Aerodynamics. GM-TR-0165-0036D, Space Tech. Labs., The Ramo-Wooldridge Corp., Apr. 7, 1958.

7. Zartarian, Garabed, Hsu, Pao Tan, and Ashley, Holt: Dynamic Airloads and Aeroelastic Problems at Entry Mach Numbers. Jour. Aerospace Sci., vol. 28, no. 3, Mar. 1961, pp. 209-222.

8. Eggers, A. J., Jr., and Savin, Raymond C.: Approximate Methods for Calculating the Flow About Nonlifting Bodies of Revolution at High Supersonic Airspeeds. NACA TN 2579, 1951.

9. Von Kármán, Th.: Isaac Newton and Aerodynamics. Jour. Aero. Sci., vol. 9, no. 14, Dec. 1942, pp. 521-522, 548.

10. Grimminger, G., Williams, E. P., and Young, G. B. W.: Lift on Inclined Bodies of Revolution in Hypersonic Flow. Jour. Aero. Sci., vol. 17, no. 11, Nov. 1950, pp. 675-690.

11. Lees, Lester: Hypersonic Flow. Preprint No. 554, S.M.F. Fund Preprint, Inst. Aero. Sci., June 1955.

12. Herr, Robert W.: A Wide-Frequency-Range Air-Jet Shaker. NACA TN 4060, 1957.

13. Bond, Reuben, and Packard, Barbara B.: Unsteady Aerodynamic Forces on a Slender Body of Revolution in Supersonic Flow. NASA TN D-859, 1961.

TABLE I.- PROPERTIES OF MODELS

[$b = 0.667$ ft; $\delta = 7.5^\circ$; and $r_b = 0.0878$ ft]

Model	$\bar{x}_\alpha$	m, lb-sec^2/ft	$\bar{x}_g$	I_α, ft-lb-sec^2	r_α^2
1	0.50	20.11×10^{-4}	0.0564	0.5225×10^{-4}	0.0585
1A	.50	21.7	.0862	.543	.0562
1B	.50	20.72	.0813	.496	.0538
2	.58	21.69	.02125	.510	.0529
3	.667	19.97	-.0496	.486	.0549
3A	.667	26.05	.0365	.764	.0659
3B	.667	20.91	.004375	.366	.0394
4	.75	23.35	-.0685	.558	.0538

TABLE II.- DRAG COEFFICIENT DATA

M	C_D	
	Average upper value	Average lower value
2	0.295	0.275
3	.19	.16
6.83	.06	.047

TABLE III.- EXPERIMENTAL RESULTS

Model	Run	f_α, cps	$\frac{m}{m_h}$	$\frac{\omega_h}{\omega_\alpha}$	f_1, cps	f_2, cps	f_f, cps	M	q, lb/ft^2	ρ, $\frac{lb\text{-}sec^2}{ft^4}$	V, ft/sec	1/k	$1/\mu$	$\frac{V}{\frac{b}{2}\omega_\alpha\sqrt{\mu}}$	$\frac{\omega_\alpha}{\omega_f}$
1	1	40.4	0.602	1.133	38.4	49.2	48	1.64	282	2.49×10^{-4}	1506	14.97	0.001995	0.796	0.842
1	2	40.25	.606	1.225	39.2	51.5	50	1.64	227.2	2.017	1501	14.33	.001616	.716	.805
1	3	40.5	.609	1.314	39.2	56.7	53	1.64	332.3	2.945	1503	13.53	.00236	.860	.764
1	4	40.4	.599	1.002	36.9	45.2	[a]----	1.64	2475	21.94	1502	-----	.0176	2.352	-----
1	5	40.4	.601	1.083	38.0	47.5	47	1.64	218.5	1.936	1504	15.25	.001554	.700	.860
1	6	40.2	.613	1.603	39.5	67.5	62.5	1.64	439	3.87	1506	11.5	.003101	.996	.6435
1	7	40.1	.6155	1.852	39.85	75.9	70	1.64	692	6.09	1508	10.28	.004885	1.255	.573
1	8	40.2	.613	1.605	39.55	67.55	62.5	1.64	428.5	3.77	1508	11.51	.00302	.984	.6435
1	9	40.1	.6175	1.994	39.9	81.6	75.5	1.64	785.5	6.91	1508	9.53	.00554	1.335	.531
1	10	40.1	.619	2.142	39.9	88.8	81	1.64	955	8.375	1510	8.90	.006715	1.474	.495
1	11	40.1	.621	2.26	39.9	93.0	87	1.64	1105	9.70	1510	8.28	.00778	1.585	.461
1	12	40.25	.600	1.035	37.4	45.65	[a]----	1.64	2492	21.9	1508	-----	.0176	2.37	-----
1	13	47.05	.615	1.585	46.7	76.2	71	1.64	595.5	5.22	1512	10.16	.004185	.992	.663
1	14	47.05	.613	1.402	46.3	68.2	65	1.64	404	3.565	1505	11.05	.00286	.817	.724
1	15	47.3	.6175	1.664	46.75	81.25	74.5	1.64	721.5	6.34	1510	9.67	.00508	1.086	.635
1	16	47.3	.619	1.811	46.75	89.1	84	1.64	895	7.84	1511	8.58	.00629	1.209	.563
2	17	40.95	.642	2.144	40.9	88.35	80	1.64	1625	14.15	1516	9.05	.01053	1.814	.512
2	18	41.55	.639	1.788	41.5	74.6	67	1.64	1127	9.89	1510	10.75	.00736	1.489	.620
2	19	41.55	.633	1.302	40.8	55.7	51	1.64	442	3.9	1506	14.07	.00290	.930	.815
2	20	40.7	.627	1.13	40.25	46.7	46	1.64	188	1.666	1503	15.58	.00124	.620	.885
2	[b]21	40.7	.6245	1.08	40.0	44.9	45	1.64	152.1	1.347	1504	15.93	.001003	.558	.904
2	[b]22	40.7	.6245	1.08	40.0	44.85	44.5	1.64	152.1	1.347	1504	16.11	.001003	.558	.914
2	23	40.4	.623	1.007	38.9	42.4	[a]----	1.64	2638	23.28	1505	-----	.01731	2.347	-----
2	24	40.3	.624	1.046	39.25	43.5	43	1.64	260.1	2.305	1504	16.67	.001715	.7365	.938
2	25	40.25	.636	1.605	40.0	65.75	60	1.64	762	6.71	1506	11.98	.00499	1.261	.671
3	26	42.1	.623	2.108	41.9	90.85	[a]----	1.64	2505	22.2	1504		.0179	2.278	-----
3	27	41.95	.620	1.787	41.65	76.9	[a]----	1.64	2481						-----
3	28	42.0	.617	1.565	41.6	67.5	[a]----	1.64							-----
3	29	42.05	.613	1.312	41.0	57.8	[a]----	1.64	2483	21.82	1508		.0177	2.275	-----
3	30	35.3	[c].612	1.592	34.95	57.75	[a]----	1.64							-----
3	31	35.4	[c].6055	1.354	34.95	49.05	[a]----	1.64	2372	20.8	1511		[c].0169	2.645	-----
3	32	41.7	[c].6055	1.151	40.55	50.1	[a]----	1.64							-----
3	33	56.5	[c].602	.748	41.6	57.95	[a]----	1.64							-----
3A	34	32.7	.612	1.535	32.3	51.9	42	1.64	1174	10.36	1509	17.15	.00643	[d]1.765	.778
4	[e]35	49.7	------	-----	-----	-----	-----	1.64	1980	17.24	1515	-----	.01192	1.587	-----
4	[e]36	41.75	------	-----	-----	-----	-----	1.64	1228	10.75	1514	-----	.00774	1.493	-----
4	[e]37	26.2	------	-----	-----	-----	-----	1.64	480.5	4.22	1510	-----	.00292	1.486	-----
4	[e]38	37.6	------	-----	-----	-----	-----	1.64	1007	8.87	1507	-----	.006135	1.497	-----
1	39	42.25	.621	1.712	41.35	77.65	68	2	719	4.98	1700	11.94	.003992	1.214	.621
1	40	42.25	.618	1.496	41.4	66.5	61	2	479.5	3.325	1700	13.3	.00267	.993	.692
1	41	41.8	.615	1.372	41.0	59.55	51	2	358.9	2.49	1698	15.88	.0020	.867	.819
1	42	41.8	.608	1.101	39.65	49.5	49	2	357.3	2.485	1697	16.52	.001993	.864	.853
1	43	42.5	.625	2.032	42.2	89.2	80	2	1130	7.74	1710	10.20	.00621	1.514	.5315
1	44	46.2	.608	.991	42.15	51.1	[a]----	2							
1	45	46.2	.610	1.027	42.85	52.1	[a]----	2	2512	17.33	1704	-----	.0139	2.075	------
1	46	42.3		1.115	40.45	50.2	50	2	299.1	2.063	1704	16.25	.001656	.781	.846

[a]Top tunnel, no flutter.
[b]Same run repeated.
[c]Based on $m = 19.87 \times 10^{-4}$ lb-sec^2/ft.
[d]Violent flutter; model destroyed.
[e]Divergence test; model free to pitch only.

TABLE III.- EXPERIMENTAL RESULTS - Concluded

Model	Run	f_α, cps	$\frac{m}{m_h}$	$\frac{\omega_h}{\omega_\alpha}$	f_1, cps	f_2, cps	f_f, cps	M	q, lb/ft^2	ρ, $\frac{lb\text{-}sec^2}{ft^4}$	V, ft/sec	1/k	$1/\mu$	$\frac{V}{\frac{b}{2}\omega_\alpha\sqrt{\mu}}$	$\frac{\omega_h}{\omega_f}$
1A	47	33.4	0.617	1.286	31.6	47.9	44	2	227.5	1.576×10^{-4}	1700	18.45	0.00117	0.834	0.759
1A	48	39.2	.615	1.126	36.2	50.0	47.5	2	297	2.052	1700	17.1	.00152	.809	.825
1A	49	45.7	.6125	.962	39.5	53.15	[a]-----	2	1635	11.56	1684	-----	.00855	1.63	-----
1A	50	45.7	.616	1.06	41.45	55.85	53.75	2	384	2.648	1705	15.14	.001965	.790	.851
1A	51	45.8	.632	1.952	45.0	96.2	88	2	1054	7.40	1690	9.17	.00548	1.302	.521
2	52	41.6	.600	2.002	41.3	85.9	75	2	1667	11.39	1713	10.89	.00848	1.809	.555
2	53	41.6	.642	1.695	41.1	73.1	65	2	1068	7.36	1705	12.51	.00548	1.448	.640
2	54	42.05	.636	1.373	42.0	57.8	57	2	418.5	2.888	1705	14.26	.00215	.897	.738
2	55	42.05	.631	1.084	40.95	47.15	46	2	146.2	1.019	1695	17.56	.000759	.5295	.914
2	56	41.9	.630	1.077	41.1	46.25	46	2	312.5	2.17	1698	17.61	.001616	.777	.911
2	57	41.9	.626	.954	39.15	42.95	[a]-----	2							
4	[e]58	41.05	------	-----	-----	-----	------	2	1061	7.3	1705	-----	.00505	1.407	-----
4	[e]59	48.55	------	-----	-----	-----	------	2	1609	11.05	1705	-----	.00765	1.475	-----
4	[e]60	37.85	------	-----	-----	-----	------	2	982	6.71	1714	-----	.00464	1.469	-----
4	[e]61	26.4	------	-----	-----	-----	------	2	579.5	3.97	1708	-----	.002749	1.615	-----
1	62	42.75	.621	1.82	42.1	82.2	75	3	866	3.945	2095	13.33	.00319	1.323	.570
1	63	42.75	.616	1.515	41.95	67.8	62	3	507.5	2.31	2095	16.1	.001873	1.011	.690
1	64	42.65	.612	1.312	41.45	59.0	51	3	251	1.16	2080	17.7	.00094	.713	.762
1	65	48.0	.616	1.333	47.2	65.95	63	3	337.1	1.541	2091	15.85	.001249	.735	.762
1	66	48.0	.612	1.165	45.9	59.75	56	3	192.6	.898	2071	17.65	.000728	.556	.857
1	67	47.25	.609	1.003	43.6	52.2	[f]-----	3	581	2.693	2078	[f]-----	.002182	.979	-----
1	68	47.25	.611	1.16	45.35	58.25	55	3	205	.954	2072	17.96	.000773	.582	.859
1	69	47.5	.611	1.151	45.4	58.45	55	3	185.5	.8625	2075	18.0	.000699	.5505	.864
2	70	42.85	.646	1.784	42.5	78.4	70	3	1202	5.395	2113	14.4	.004015	1.491	.612
2	71	42.85	.642	1.48	42.5	64.5	60	3	676	3.06	2101	16.7	.00228	1.116	.714
2	72	42.3	.638	1.32	41.8	57.0	53	3	398	1.831	2085	18.76	.001364	.868	.798
2	73	42.3	.635	1.095	41.3	47.8	845	3	22.57	.1078	2048	21.7	.0000803	.2065	.941
2	74	48.0	.642	1.313	47.9	63.2	60	3	431.5	1.959	2100	16.69	.001459	.796	.800
2	75	48.0	.638	1.148	47.1	56.55	54	3	178.1	.834	2070	18.29	.000621	.514	.888
2	76	57.4	.642	1.087	56.4	63.65	59	3	101.7	.4805	2058	16.61	.000358	.3235	.973
2	77	57.4	.636	.943	53.1	58.65	[a]-----	3	1417	6.24	2132	------	.00465	1.209	-----
2	78	56.55	.638	1.008	54.15	58.75	57.5	3	251.5	1.116	2080	17.25	.000864	.516	.983
4	[e]79	28.8	------	-----	-----	-----	------	3	718	3.343	2075	------	.002325	1.655	-----
4	[e]80	39.45	------	-----	-----	-----	------	3	790	3.655	2080	------	.00254	[h]1.267	-----
4	[e]81	32.5	------	-----	-----	-----	------	3	909	4.10	2105	------	.00285	1.645	-----
4	[e]82	38.15	------	-----	-----	-----	------	3	1220	5.55	2100	------	.00386	1.631	-----
1B	83	47.6	.618	1.64	45.0	95.0	81.8	[i]6.83	1049	.616	5845	34.1	.0004765	1.280	.582
1B	84	39.5	.619	2.138	38.5	97.1	83.35	[i]6.83	1372	.8035	5840	33.5	.0006235	1.764	.474
1B	85	37.6	.606	1.585	37.5	60.0	51.6	[i]6.83	242.1	.1277	6160	57.1	.0000991	.781	.729
1B	86	45.3	.599	.959	38.9	52.9	51.7	[i]6.83	380	.199	6180	57.1	.0001548	.812	.876
1B	87	53.9	.616	1.742	52.9	100.0	85.7	[i]6.83	1153	.7062	5715	31.85	.000548	1.185	.629
1B	88	55.1	.603	.951	47.1	64.3	64.3	[i]6.83	1384	.856	5685	42.25	.000664	1.273	.857
3B	89	53.1	.617	1.45	50.0	90.2	[a]-----	[i]6.83	2963	1.95	5505	------	.001502	1.92	-----
3B	90	45.4	.618	1.981	45.2	91.8	[a]-----	[i]6.83	4380	2.945	5455	------	.00227	2.733	-----
3B	91	44.8	.605	1.227	44.9	54.8	50.0	[i]6.83	496	.281	5940	56.8	.000216	.932	.896
2	92	40.9	.638	1.39	40.8	56.8	52.3	[i]15.4	401.6	.2143	6120	55.85	.0001595	.902	.782

[a]Top tunnel, no flutter.
[e]Divergence test; model free to pitch only.
[f]No flutter; sustained nondivergent oscillation.
[g]Flutter difficult to distinguish from transient oscillations due to starting shock of tunnel.
[h]This run not as clearly defined as other divergence runs.
[i]Helium the test medium for this Mach number.

TABLE IV.- AERODYNAMIC COEFFICIENTS IN FLUTTER ANALYSIS OF SPRING-MOUNTED CONE FOR FOUR AERODYNAMIC THEORIES

Aerodynamic coefficient	Theory			
	Munk-Jones	Frequency expansion[b]	Quasi-steady	Shock expansion[a]
A_{hh}	$\frac{1}{3} - i\frac{1}{2k}$	$-\frac{1}{2k^2}\beta \tan\delta\left(L_1 + ikL_2\right)$	$-i\frac{F}{\delta}\frac{1}{4k}$	$-i\frac{0.4825}{M\delta}\frac{1}{k}$
$A_{h\alpha}$	$\frac{1}{4} - \frac{\bar{x}_\alpha}{3} - \frac{1}{4k^2} - i\frac{1}{2k}\left(\frac{4}{3} - \bar{x}_\alpha\right)$	$-\frac{1}{2k^2}\beta \tan\delta\left(L_3 + ikL_4\right)$	$-\frac{F}{2\delta}\left[\frac{1}{4k^2} + i\frac{1}{k}\left(\frac{1}{3} - \frac{\bar{x}_\alpha}{2}\right)\right]$	$-\frac{0.4825}{M\delta}\left[\frac{1}{2k^2} - i\frac{1}{k}\left(\bar{x}_\alpha - 1.048\right)\right]$
$A_{\alpha h}$	$\frac{1}{4} - \frac{\bar{x}_\alpha}{3} - i\frac{1}{2k}\left(\frac{2}{3} - \bar{x}_\alpha\right)$	$-\frac{1}{2k^2}\beta \tan\delta\left(M_1 + ikM_2\right)$	$-i\frac{F}{\delta}\frac{1}{2k}\left(\frac{1}{3} - \frac{\bar{x}_\alpha}{2}\right)$	$-i\frac{0.4825}{M\delta}\frac{2}{k}\left(\frac{1}{3} - \frac{\bar{x}_\alpha}{2}\right)$
$A_{\alpha\alpha}$	$\frac{1}{5} - \frac{\bar{x}_\alpha}{3}\left(\frac{3}{2} - \bar{x}_\alpha\right) - \frac{1}{4k^2}\left(\frac{2}{3} - \bar{x}_\alpha\right) - i\frac{1}{2k}\left(1 - \bar{x}_\alpha\right)^2$	$-\frac{1}{2k^2}\beta \tan\delta\left(M_3 + ikM_4\right)$	$-\frac{F}{4\delta}\left[\frac{1}{k^2}\left(\frac{1}{3} - \frac{\bar{x}_\alpha}{2}\right) + i\frac{1}{k}\left(\frac{1}{2} - \frac{4}{3}\bar{x}_\alpha + \bar{x}_\alpha^2\right)\right]$	$-\frac{0.4825}{M\delta}\left[\frac{1}{k^2}\left(\frac{1}{3} - \frac{\bar{x}_\alpha}{2}\right) + i\frac{3.144}{k}\left(\frac{1}{4} - \frac{\bar{x}_\alpha}{3}\right) - i\frac{2\bar{x}_\alpha}{k}\left(\frac{1}{3} - \frac{\bar{x}_\alpha}{2}\right)\right]$

[a]Coefficients in this column based on $M = 6.83$ and $\gamma = \frac{5}{3}$ (for helium).

[b]See reference 3 for detailed expressions of L and M.

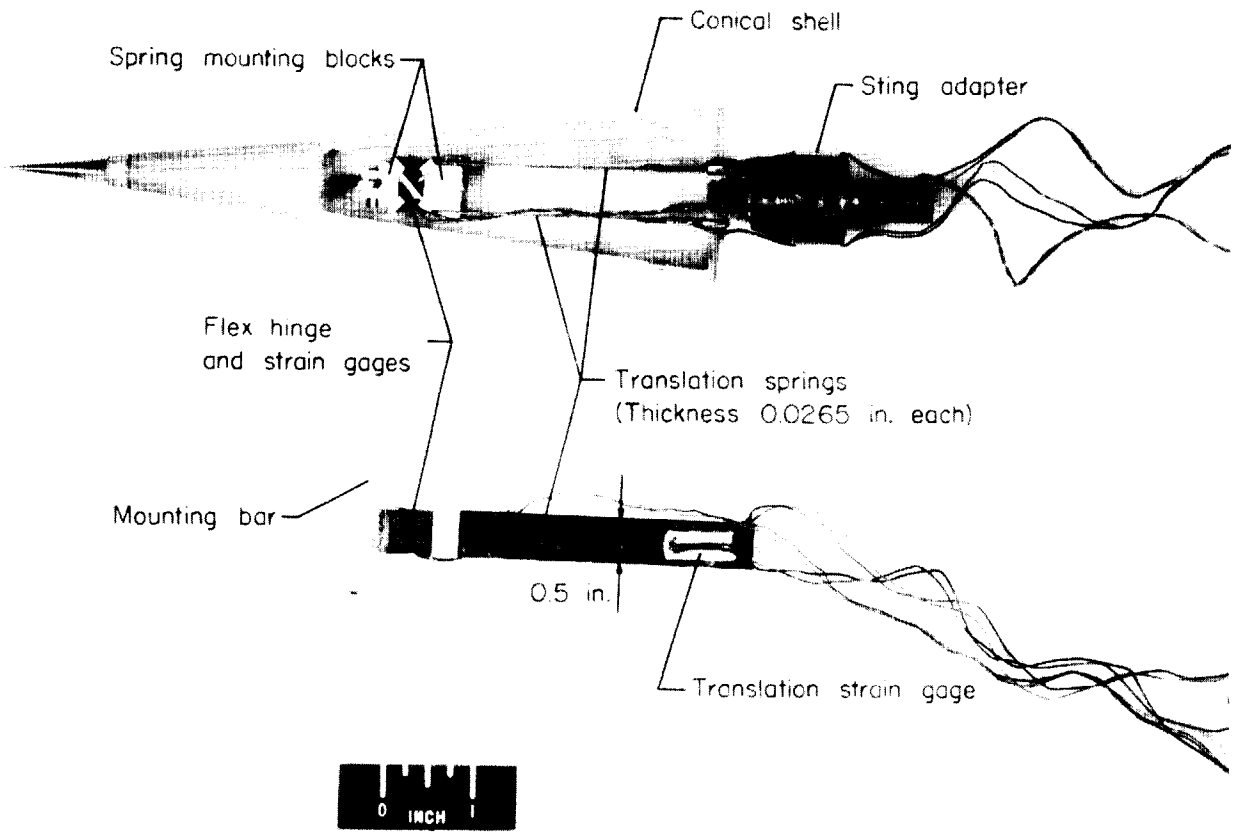

(a) Photograph with part of cone shell removed to show spring apparatus. L-60-8254

Figure 1.- Cone flutter model.

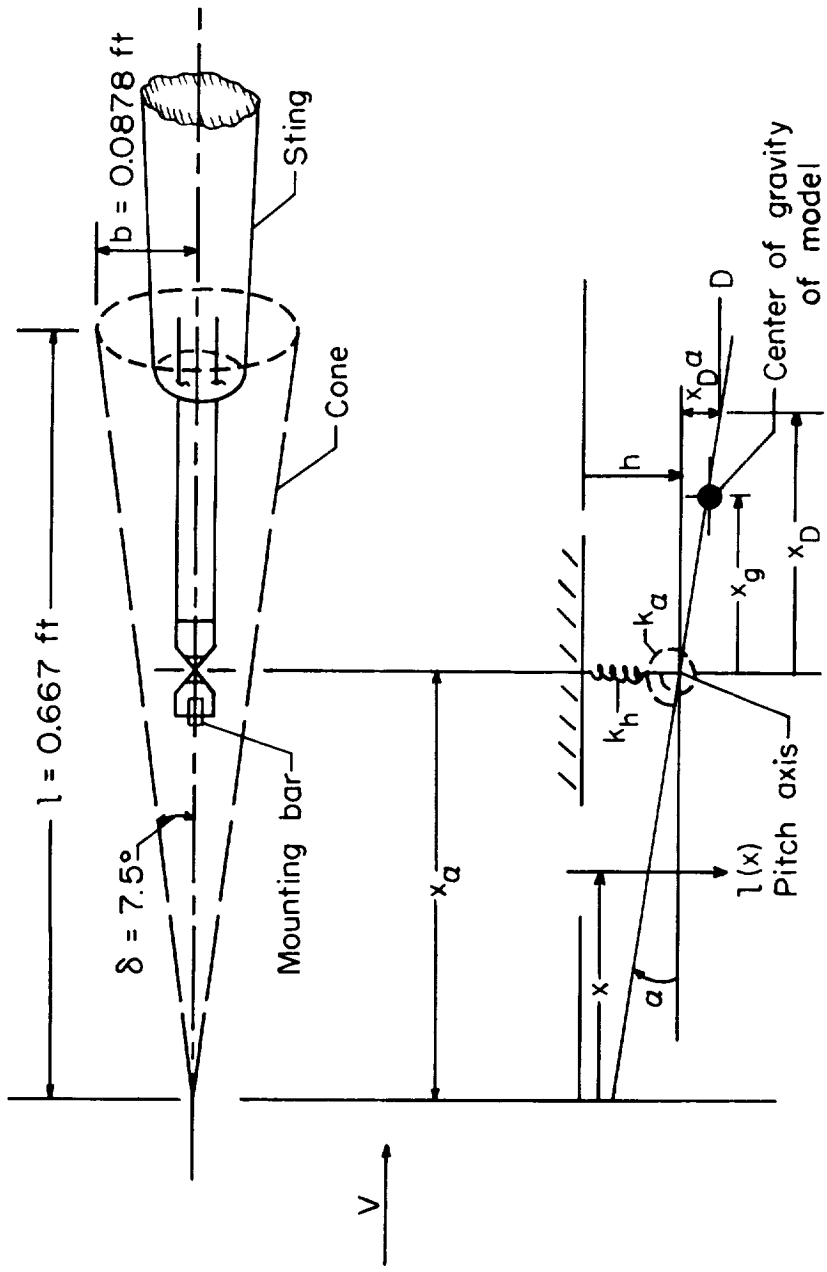

(b) Schematic view of model and spring apparatus. All directions indicated are considered positive.

Figure 1.- Concluded.

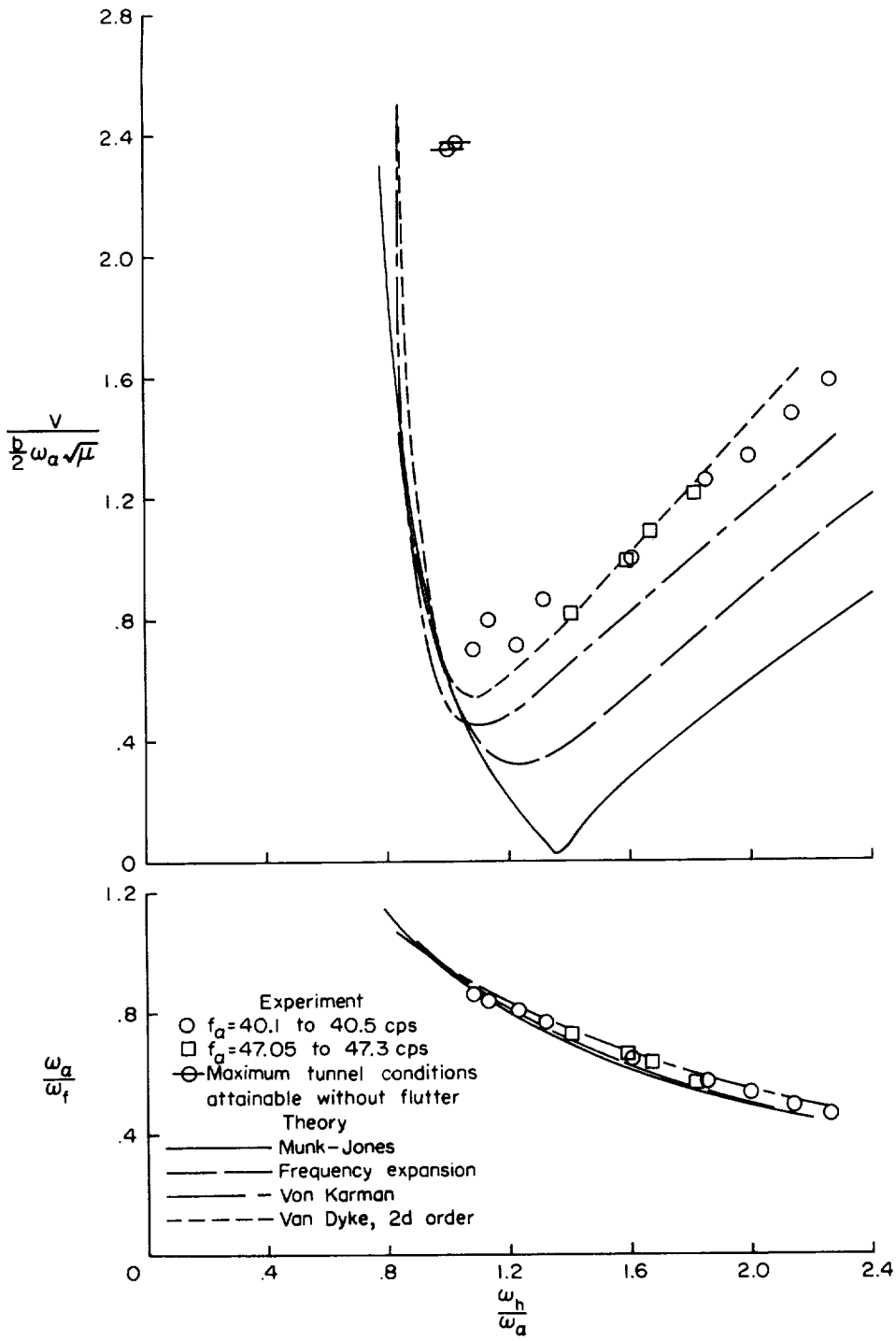

Figure 2.- Flutter boundaries for model 1 ($\bar{x}_\alpha$ = 0.50) at a Mach number of 1.64.

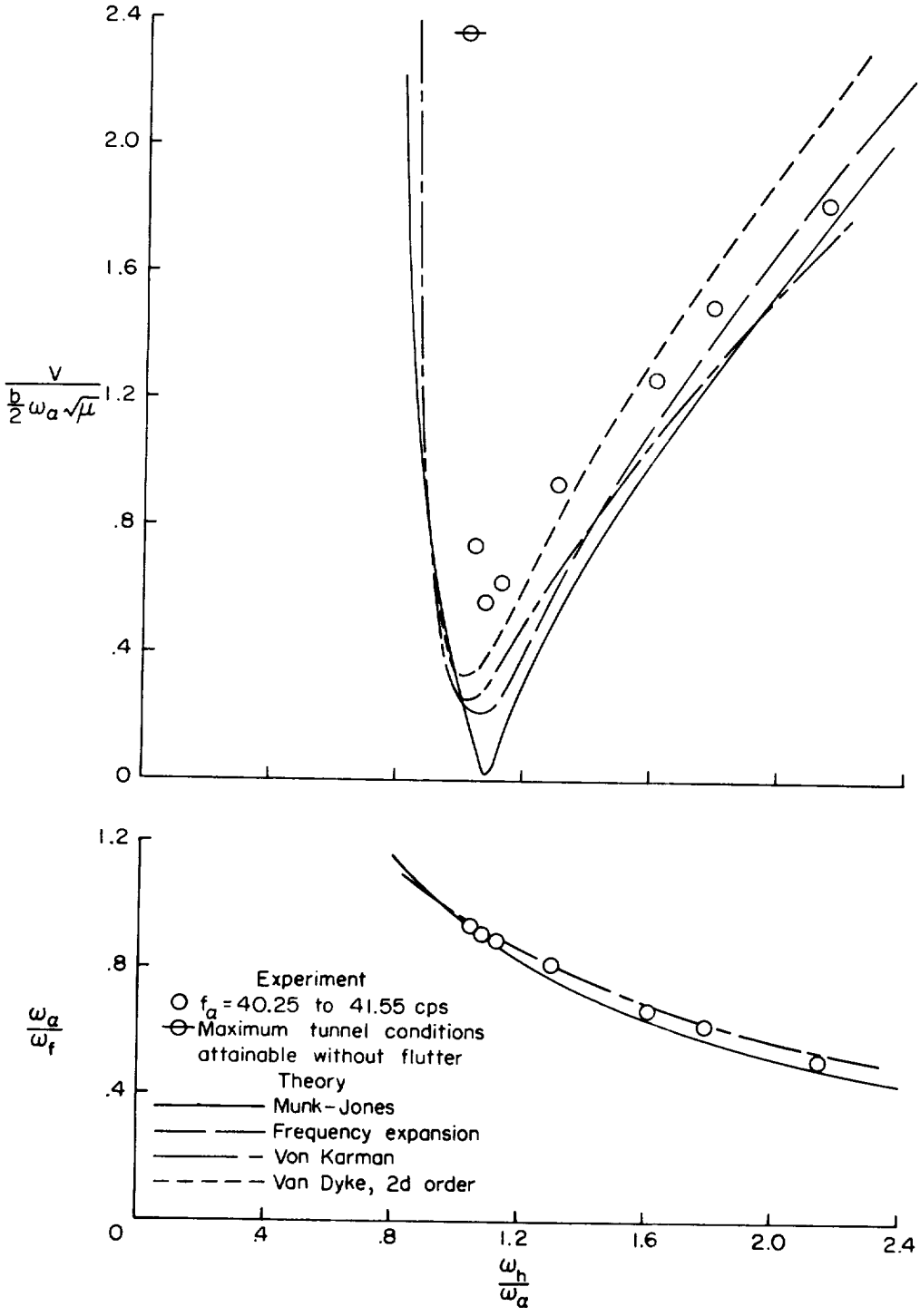

Figure 3.- Flutter boundaries for model 2 ($\bar{x}_\alpha = 0.58$) at a Mach number of 1.64.

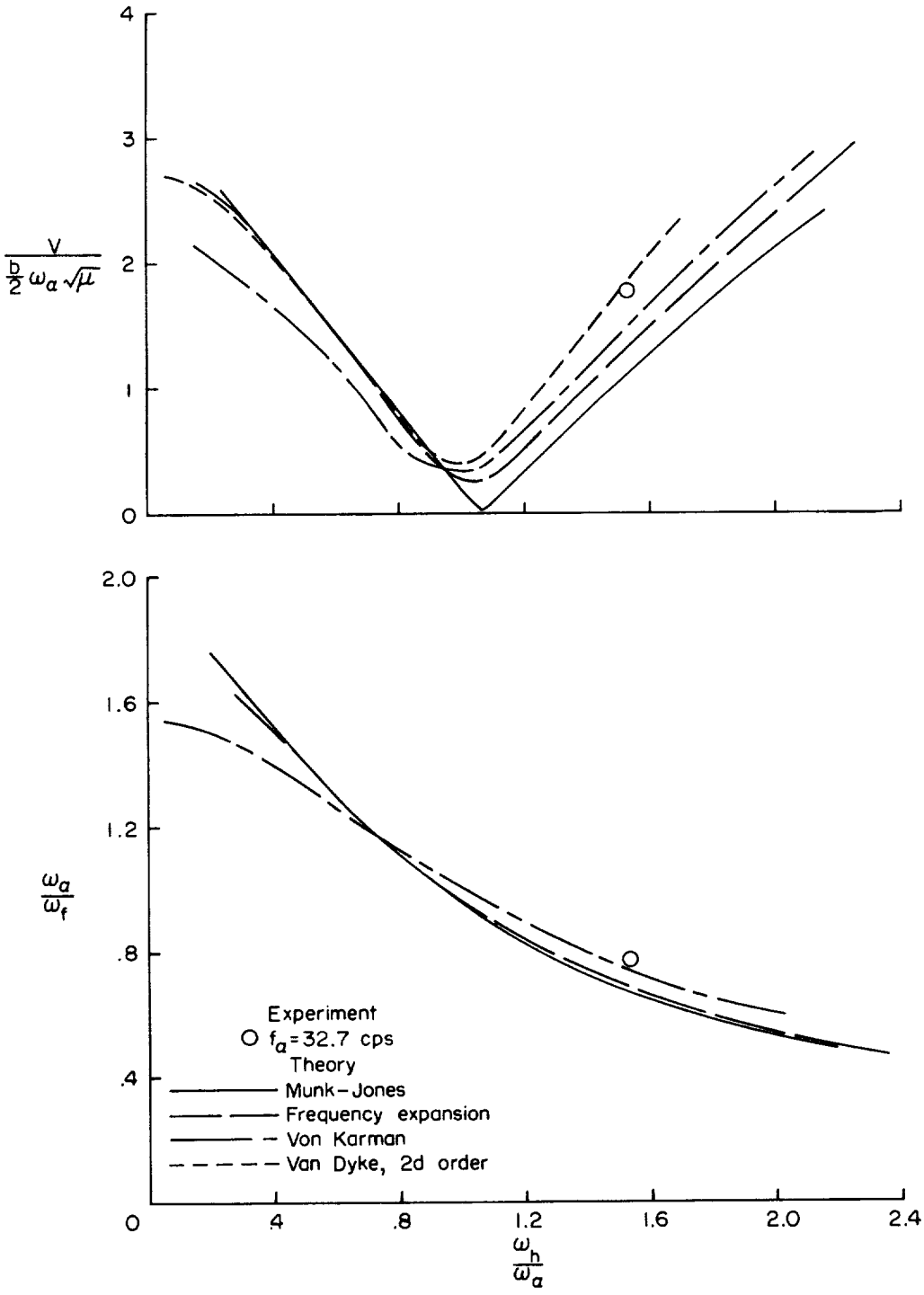

Figure 4.- Flutter boundaries for model 3A ($\bar{x}_\alpha$ = 0.667) at a Mach number of 1.64.

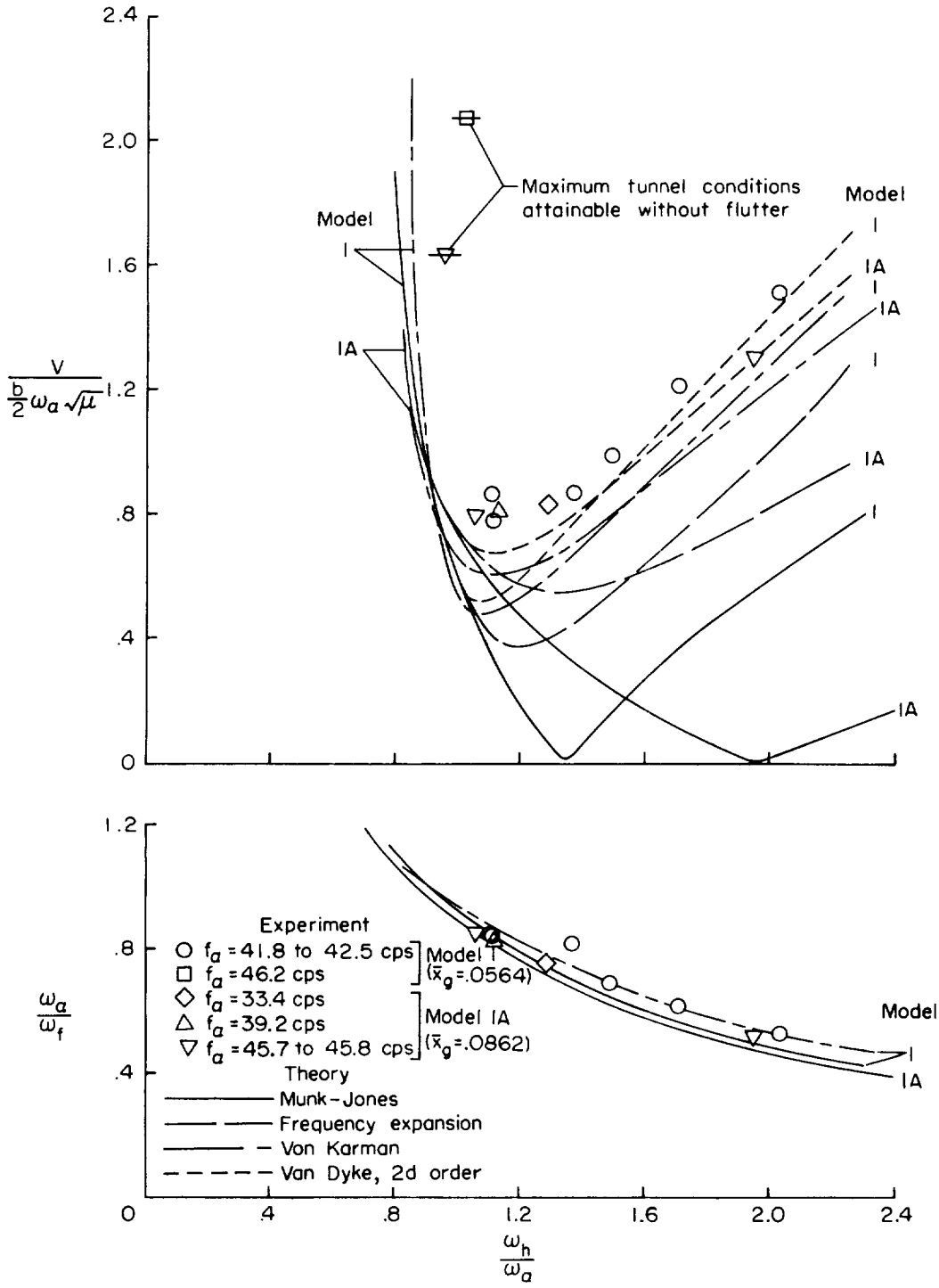

Figure 5.- Flutter boundaries for models 1 and 1A ($\bar{x}_\alpha$ = 0.50 for both models) at a Mach number of 2.

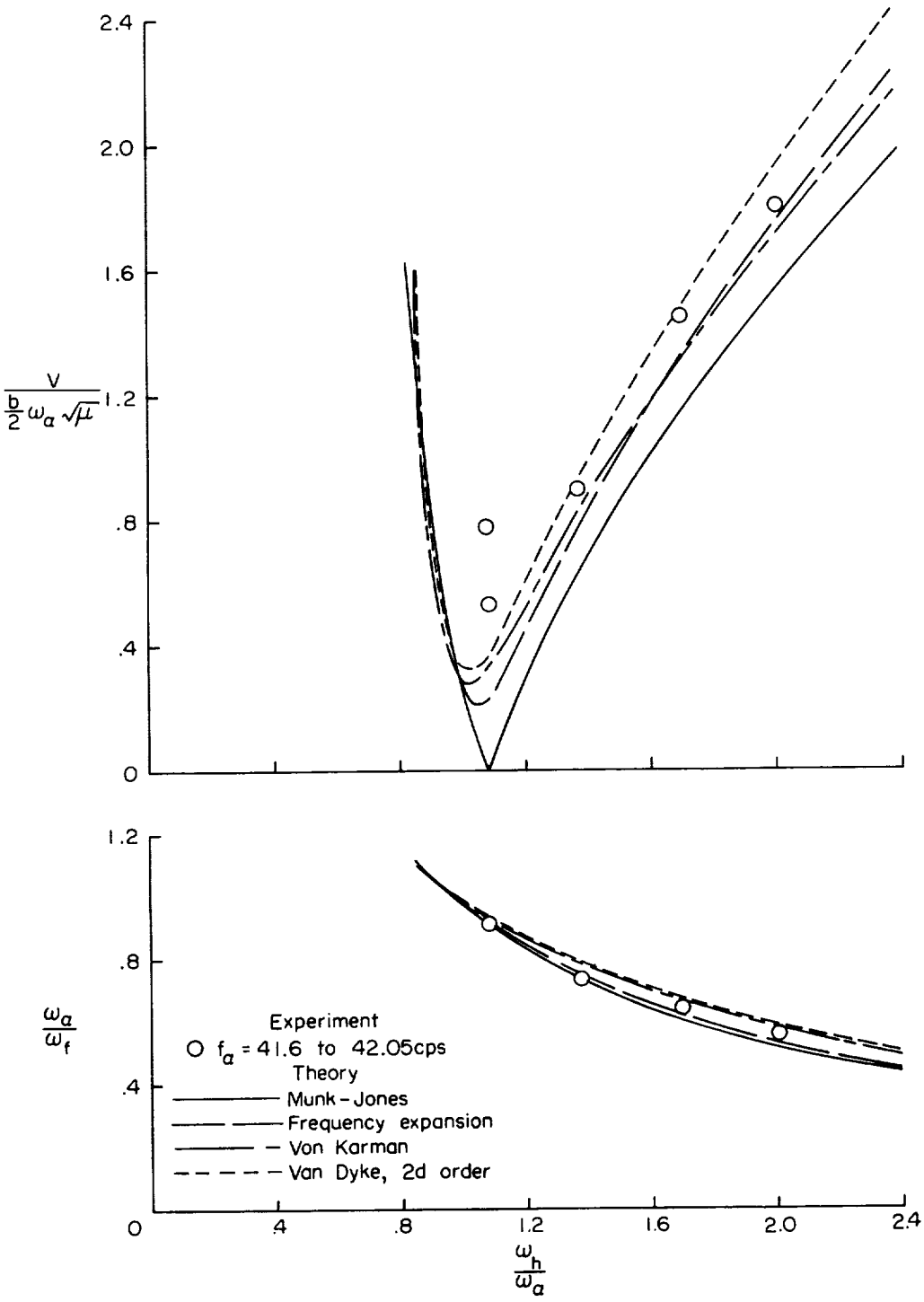

L-1262

Figure 6.- Flutter boundaries for model 2 ($\bar{x}_\alpha$ = 0.58) at a Mach number of 2.

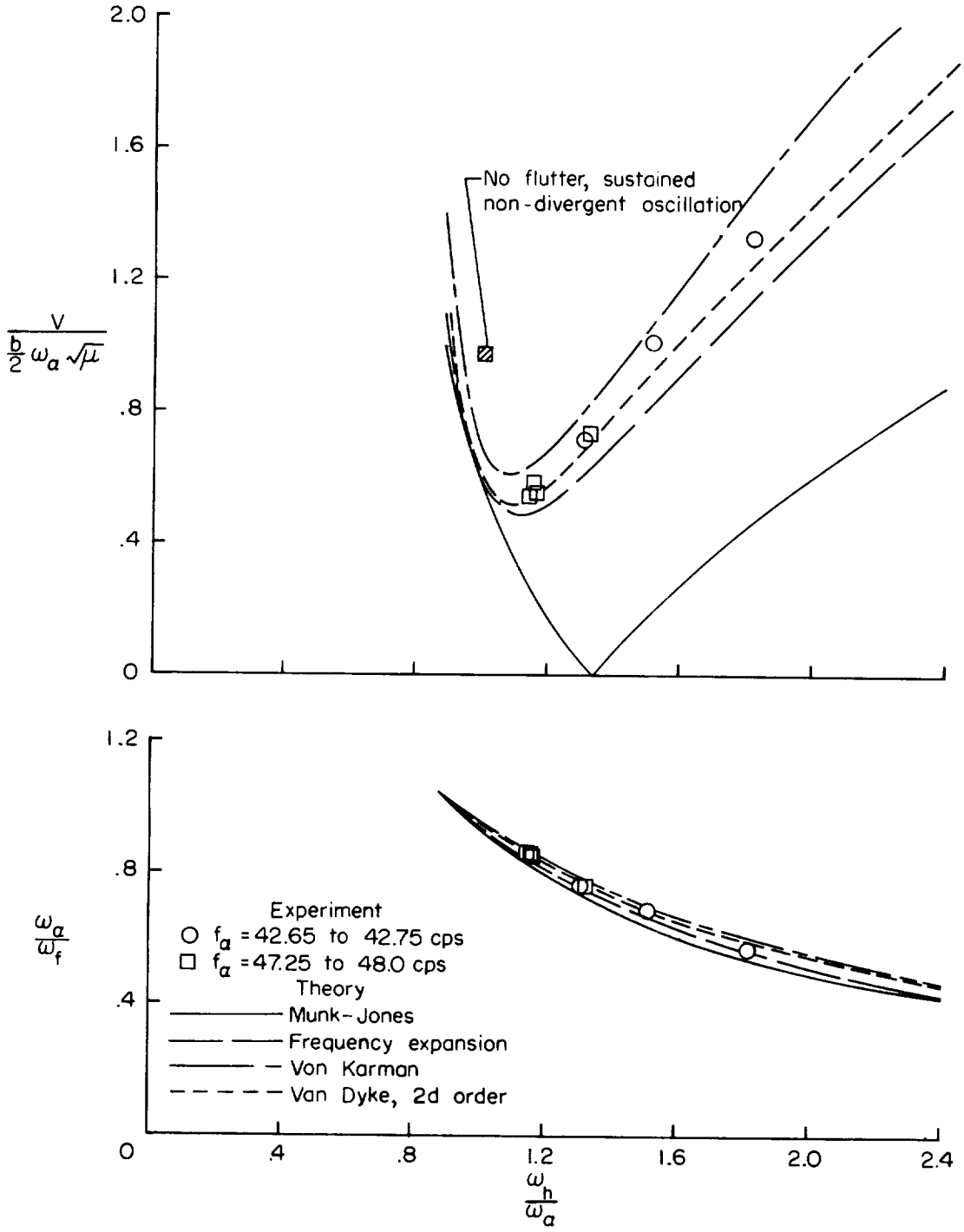

Figure 7.- Flutter boundaries for model 1 ($\bar{x}_\alpha = 0.50$) at a Mach number of 3.

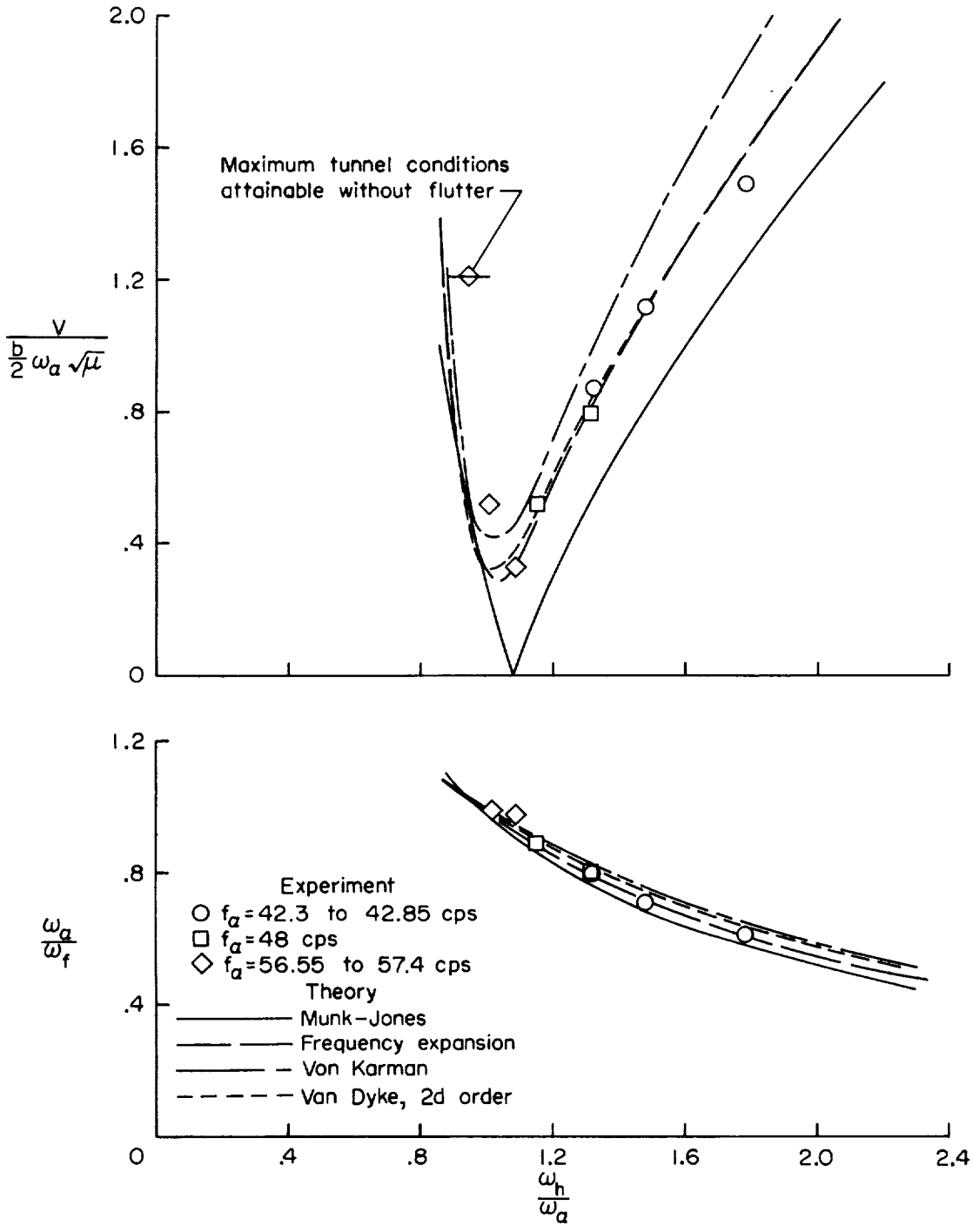

Figure 8.- Flutter boundaries for model 2 ($\bar{x}_\alpha$ = 0.58) at a Mach number of 3.

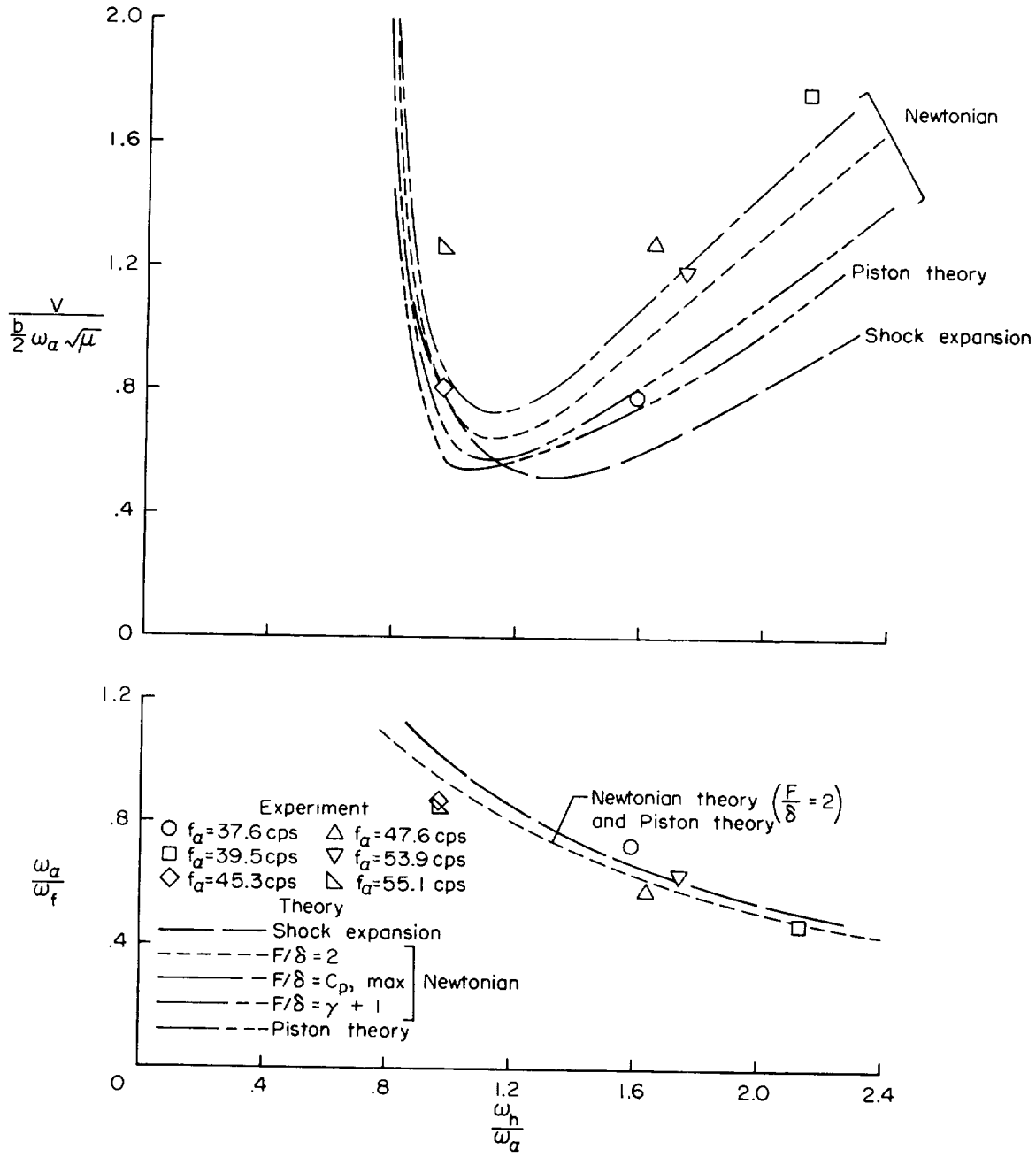

Figure 9.- Flutter boundaries for model 1B ($\bar{x}_\alpha$ = 0.50) at a Mach number of 6.83.

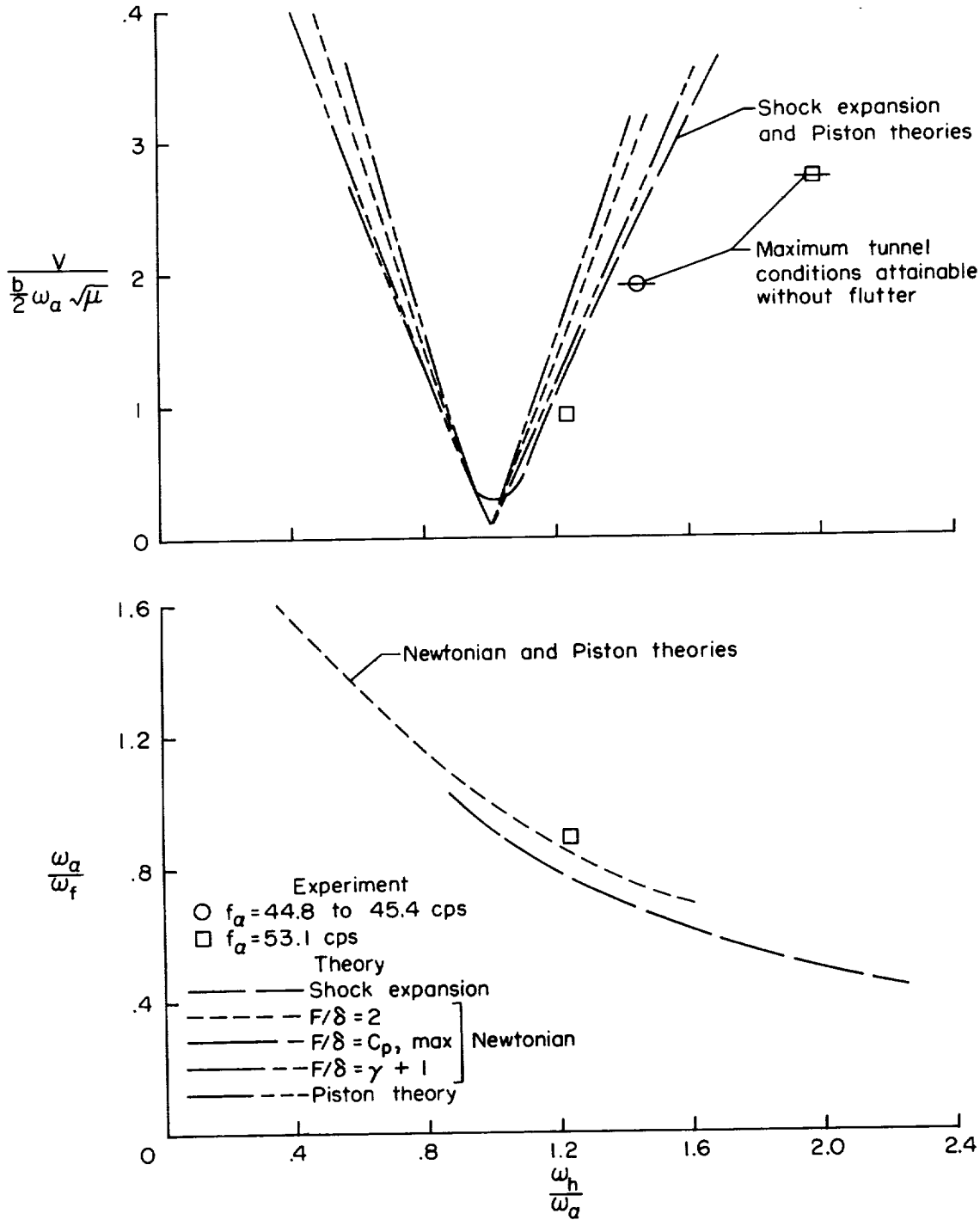

Figure 10.- Flutter boundaries for model 3B ($\bar{x}_\alpha$ = 0.667) at a Mach number of 6.83.

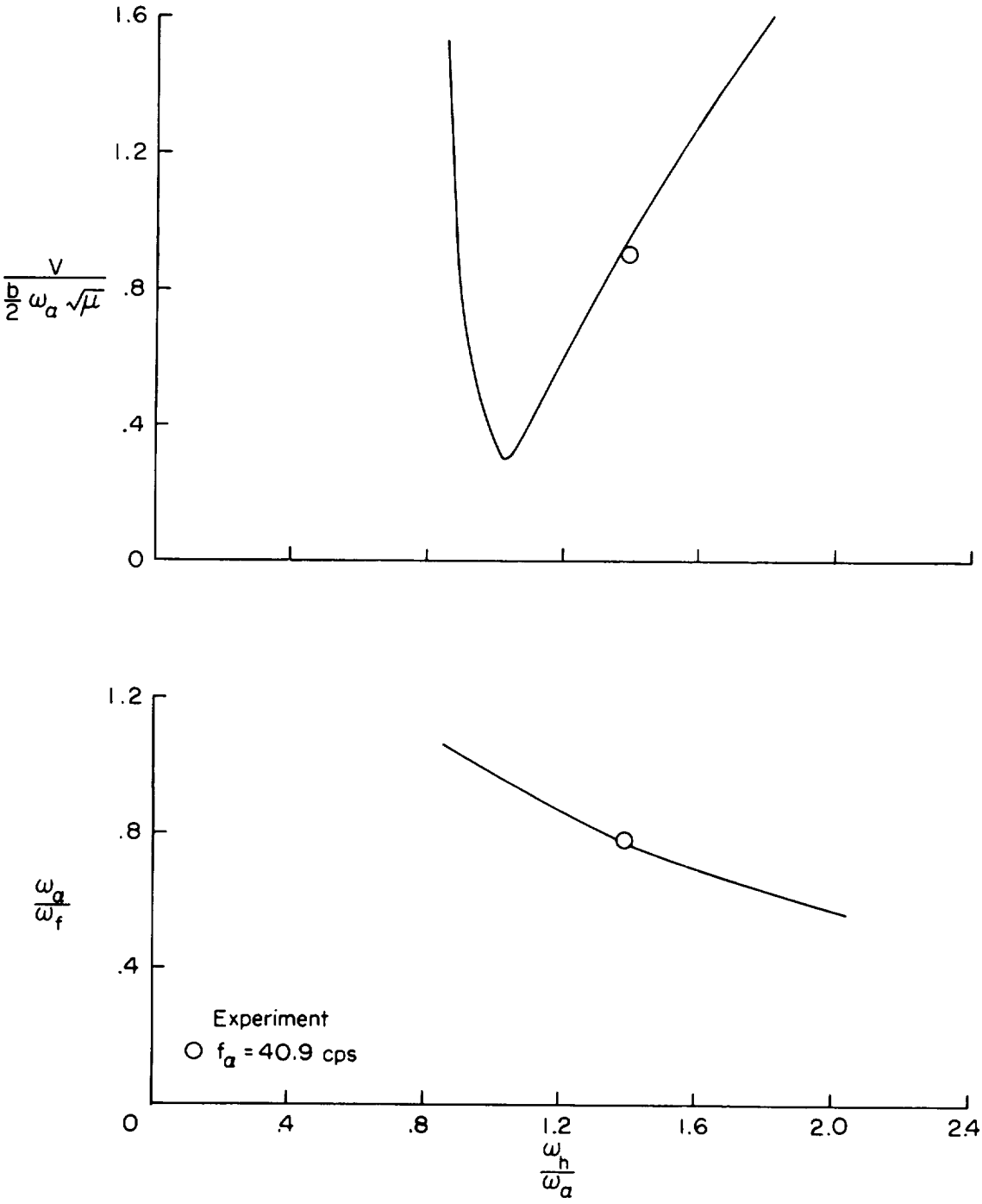

Figure 11.- Newtonian theory flutter boundary ($F/\delta = 2$) for model 2 ($\bar{x}_\alpha = 0.58$) and comparison with experiment at a Mach number of 15.4.

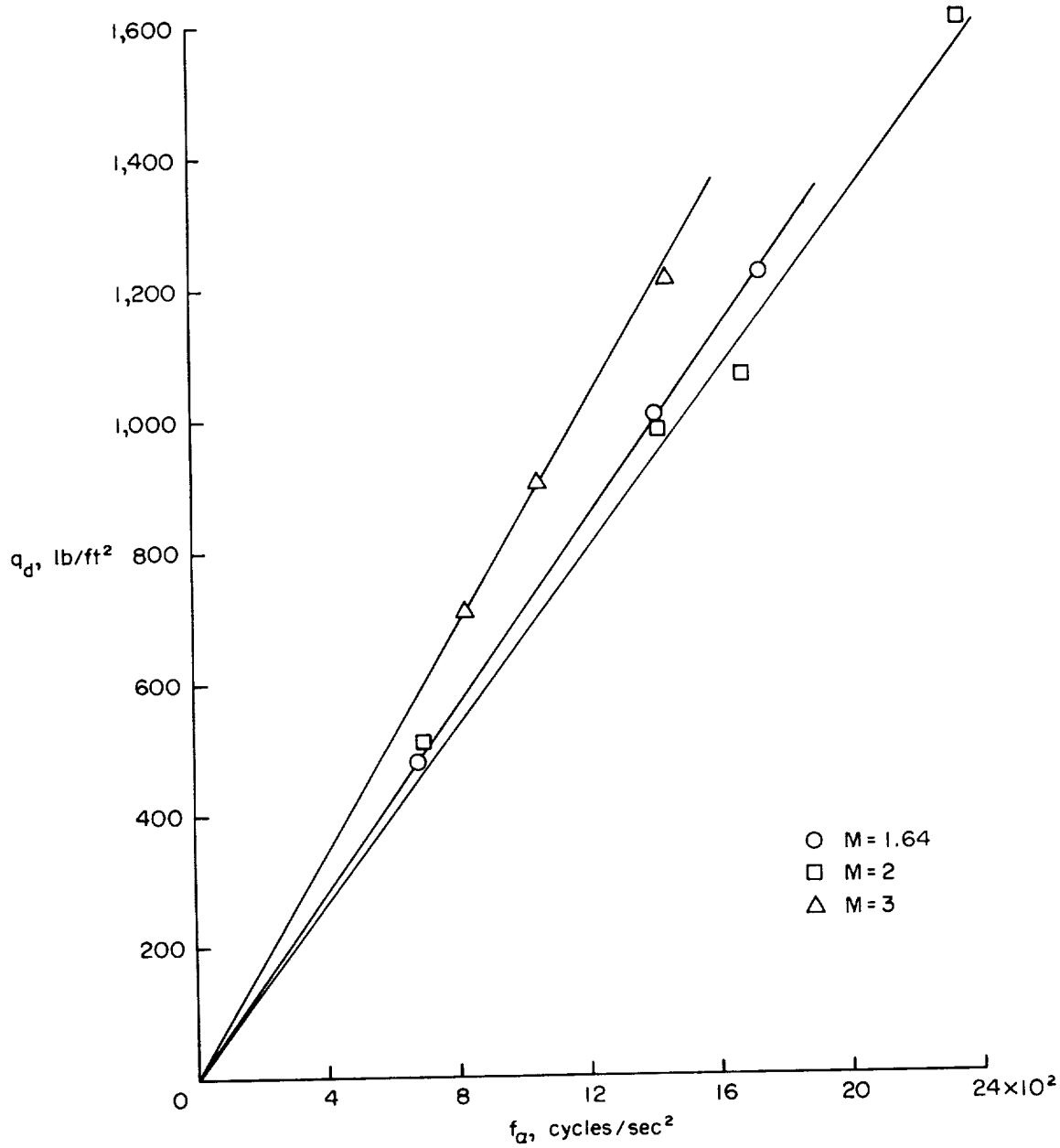

Figure 12.- Experimental divergence characteristics of model 4 ($\bar{x}_\alpha = 0.75$) at Mach numbers of 1.64, 2, and 3.

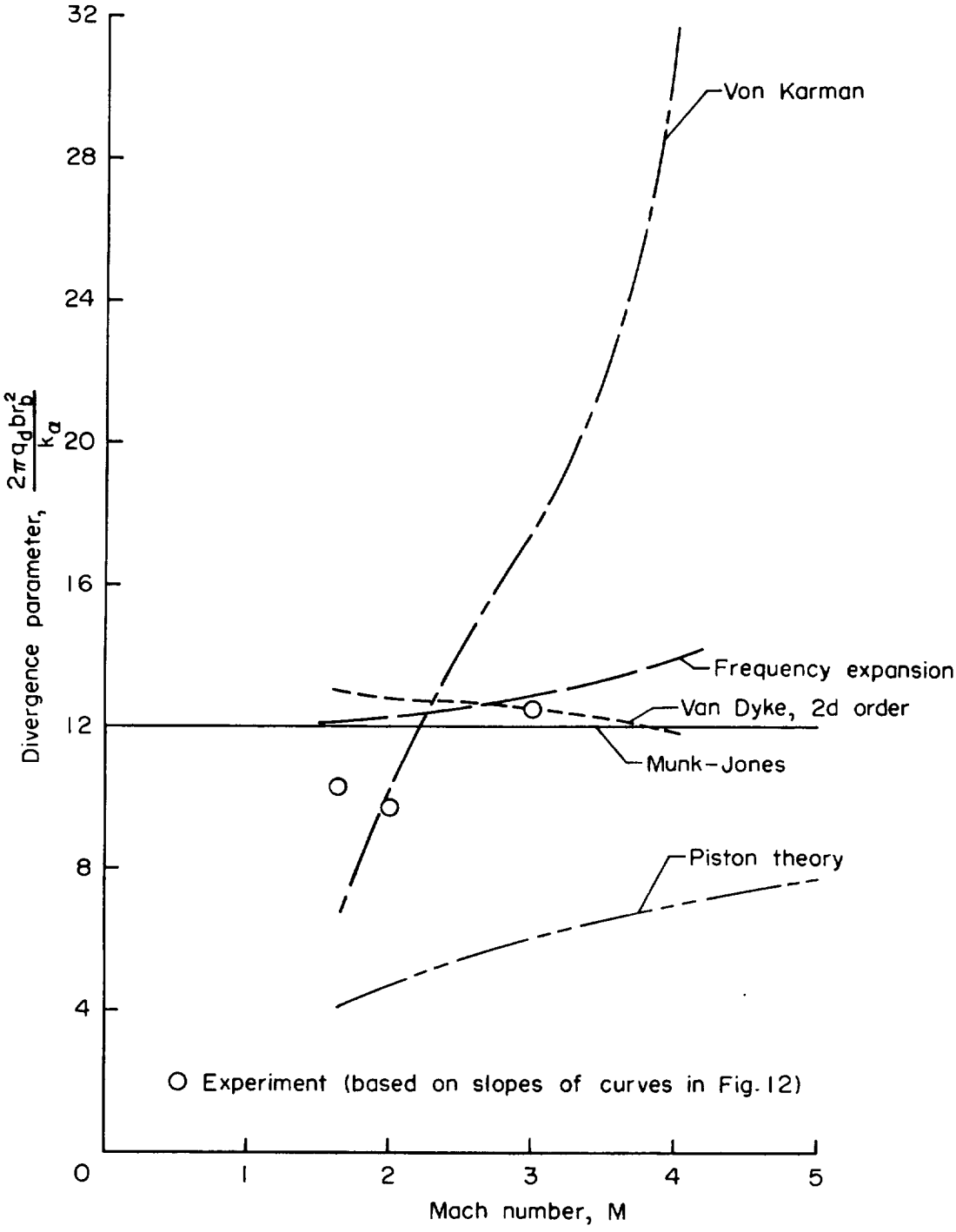

Figure 13.- Comparison of experimental and theoretical divergence parameters for model 4 ($\bar{x}_\alpha = 0.75$).

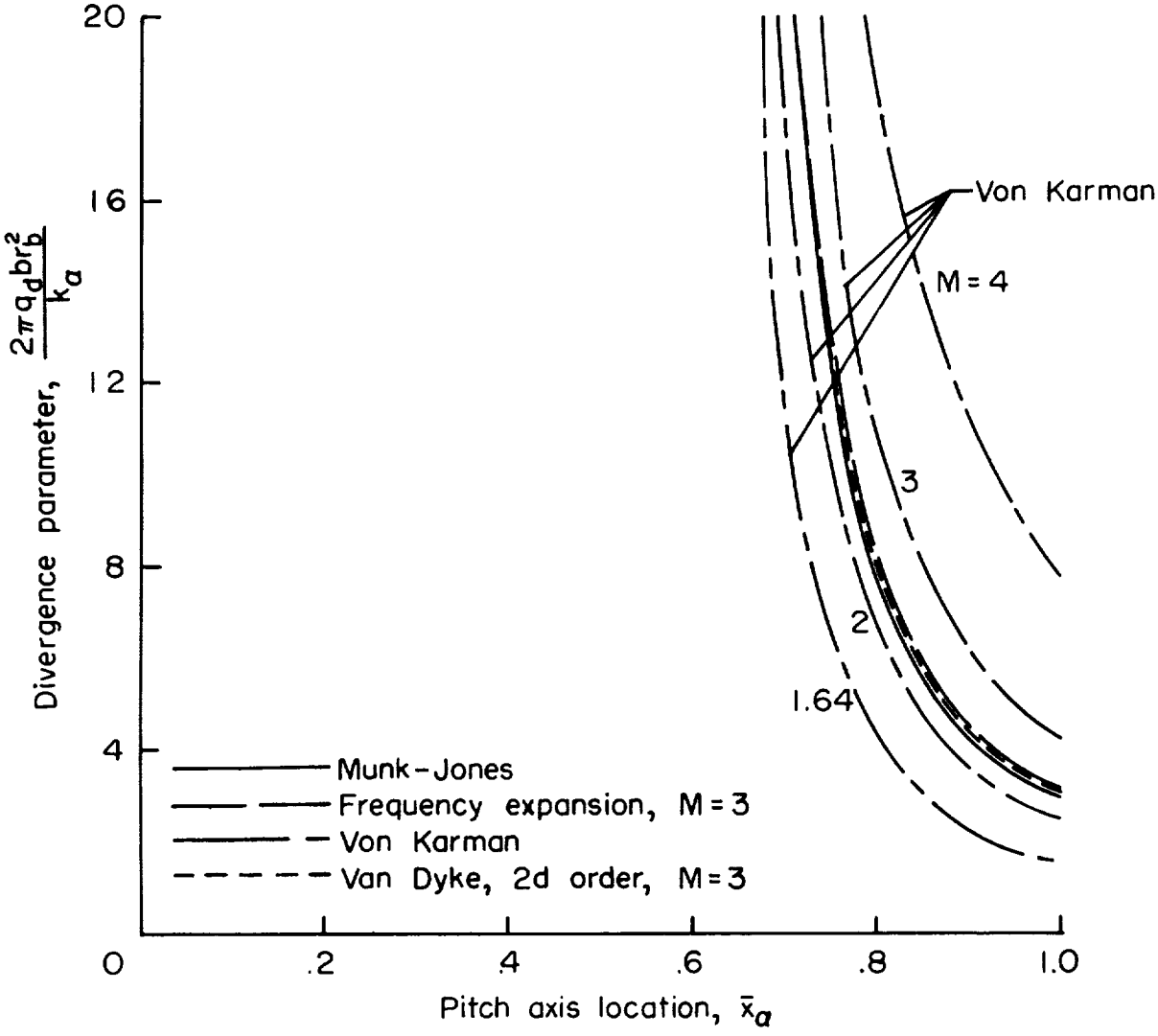

Figure 14.- Theoretical divergence boundaries of spring-mounted cone.

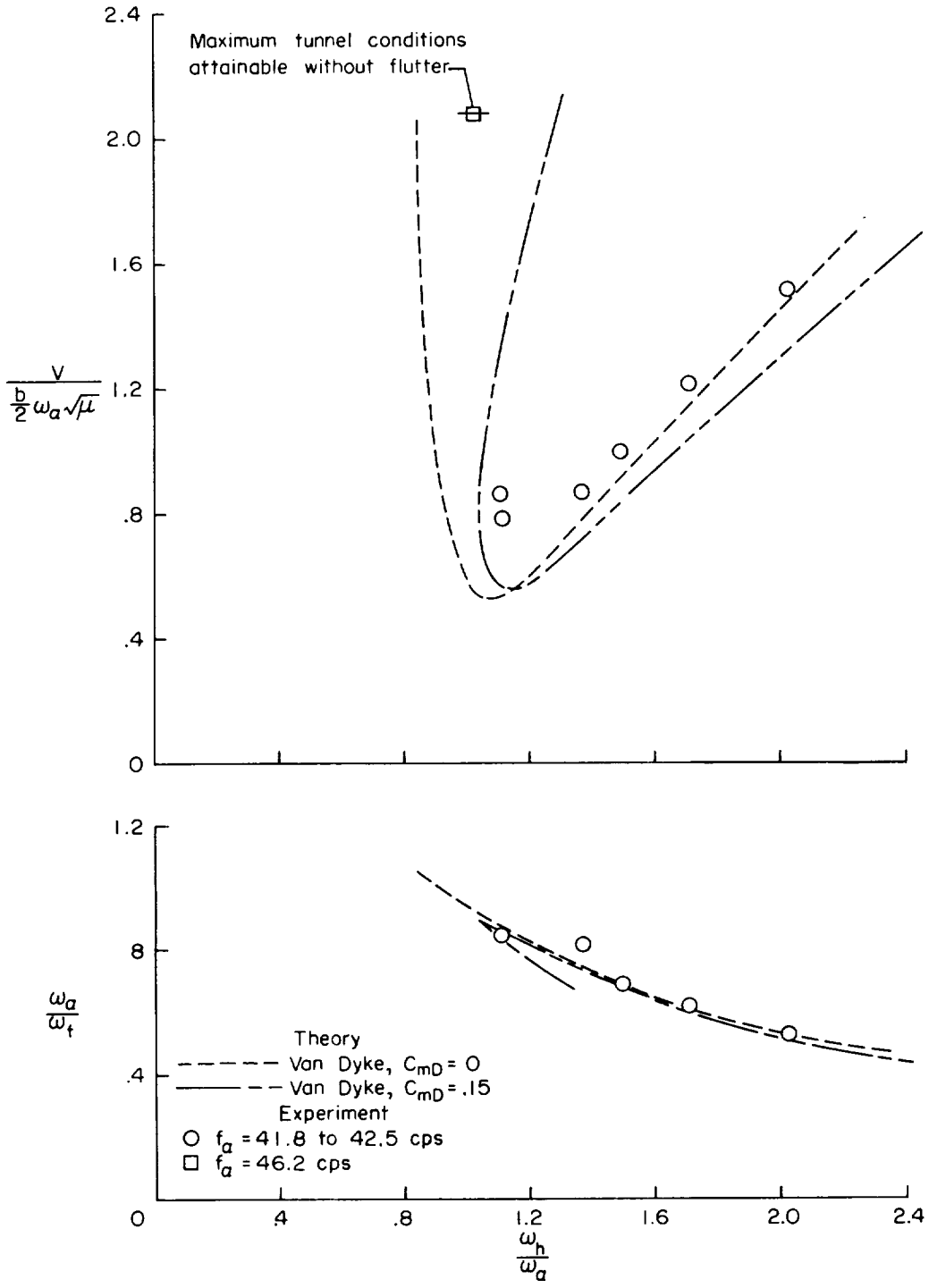

Figure 15.- Effects of steady axial force on the flutter boundaries of model 1 ($\bar{x}_\alpha$ = 0.50) at a Mach number of 2.

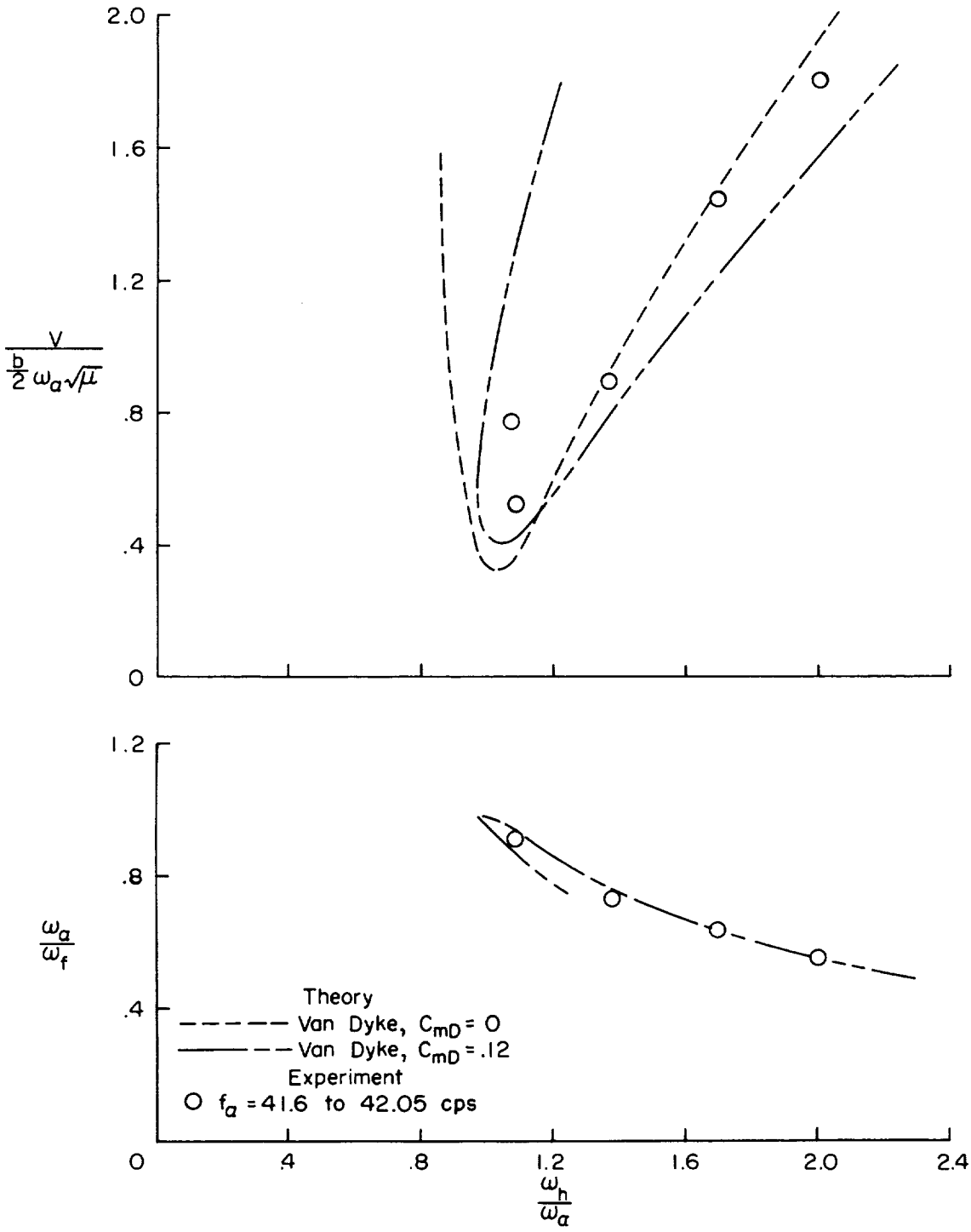

Figure 16.- Effects of steady axial force on the flutter boundaries of model 2 ($\bar{x}_\alpha = 0.58$) at a Mach number of 2.

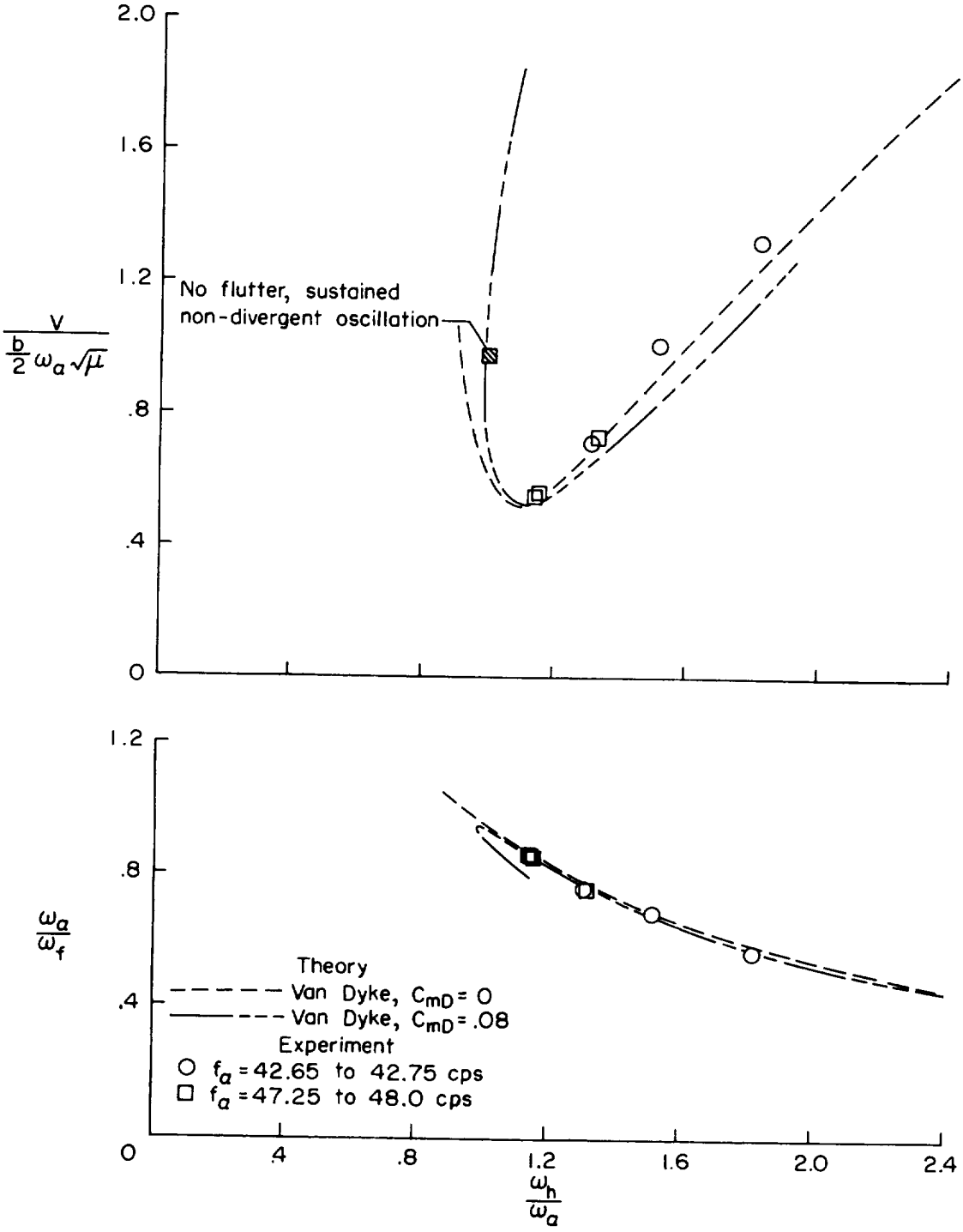

Figure 17.- Effects of steady axial force on flutter boundaries of model 1 ($\bar{x}_\alpha$ = 0.5) at a Mach number of 3.

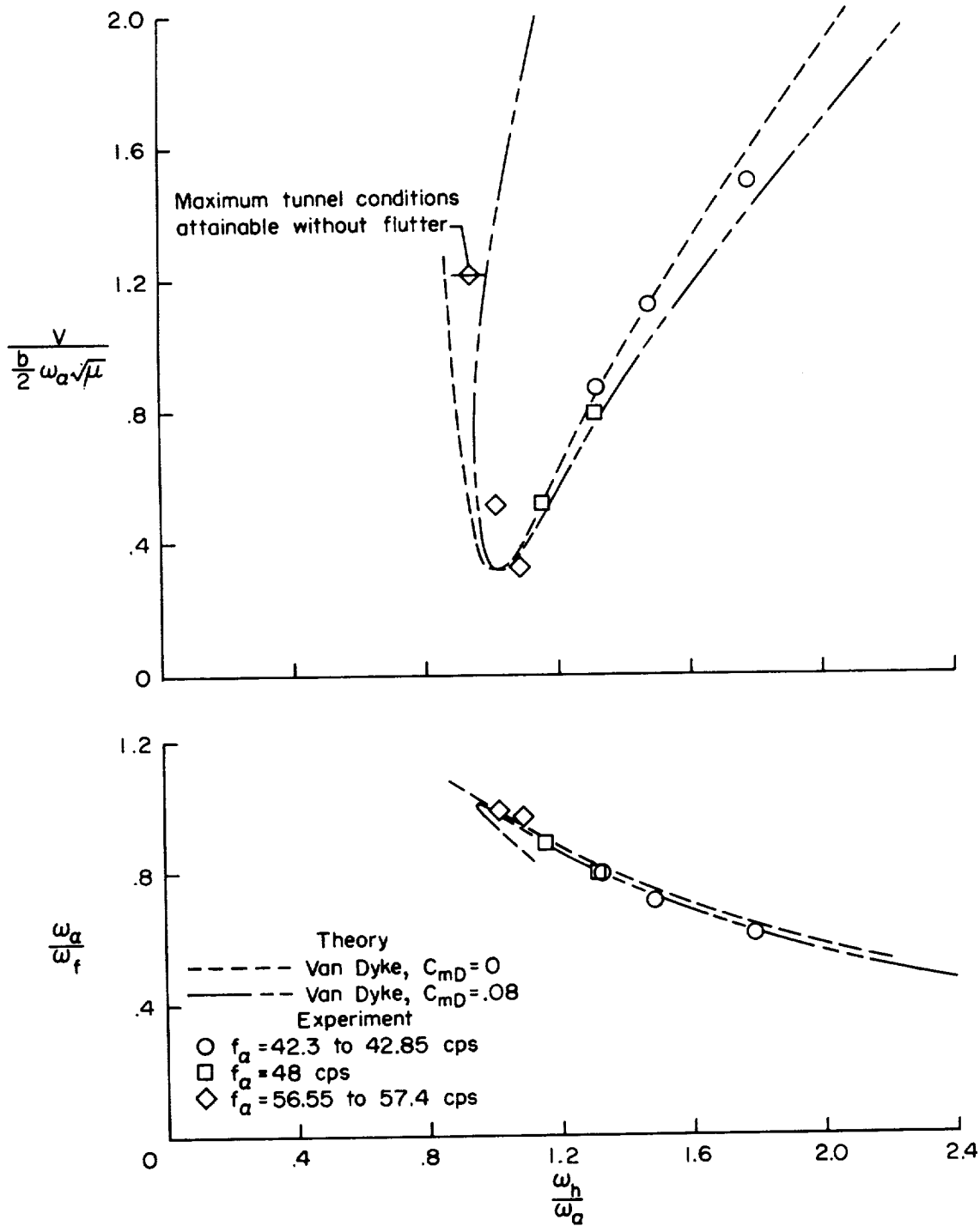

Figure 18.- Effects of steady axial force on flutter boundaries of model 2 ($\bar{x}_\alpha$ = 0.58) at a Mach number of 3.

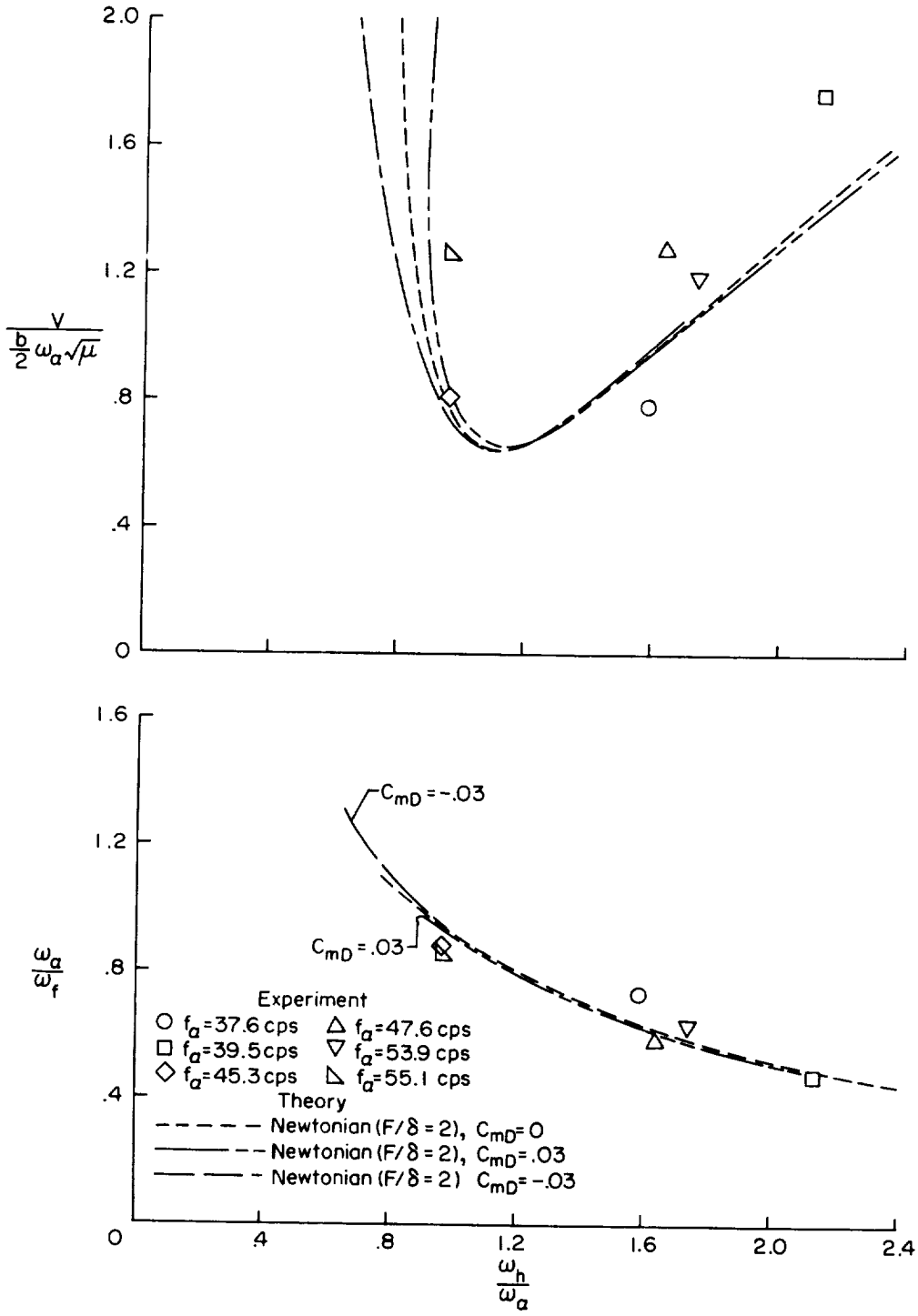

Figure 19.- Effects of steady axial force on flutter boundaries of model 1B ($\bar{x}_\alpha$ = 0.5) at a Mach number of 6.83.

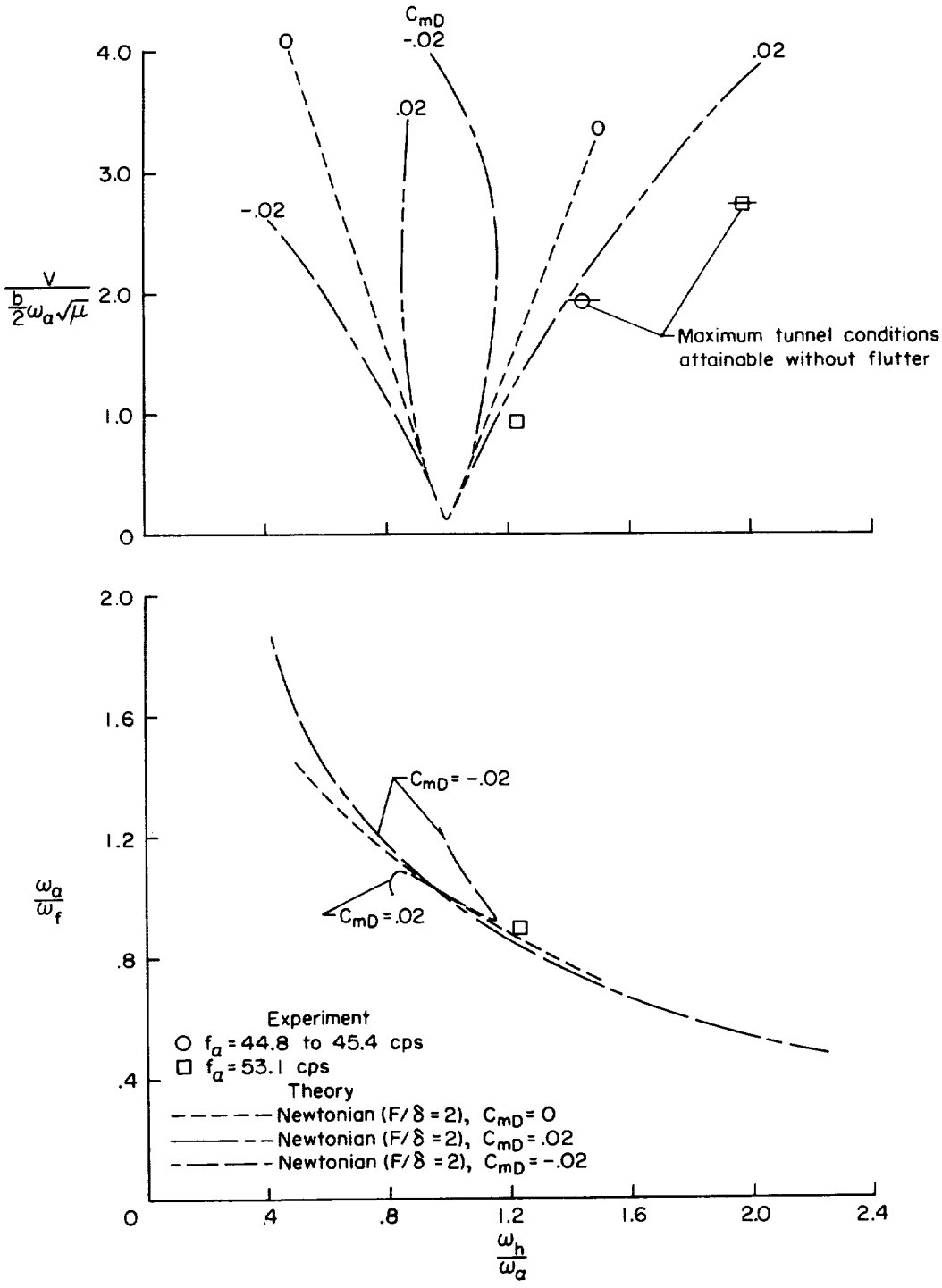

Figure 20.- Effect of steady axial force on flutter boundaries of model 3B ($\bar{x}_\alpha$ = 0.667) at a Mach number of 6.83.

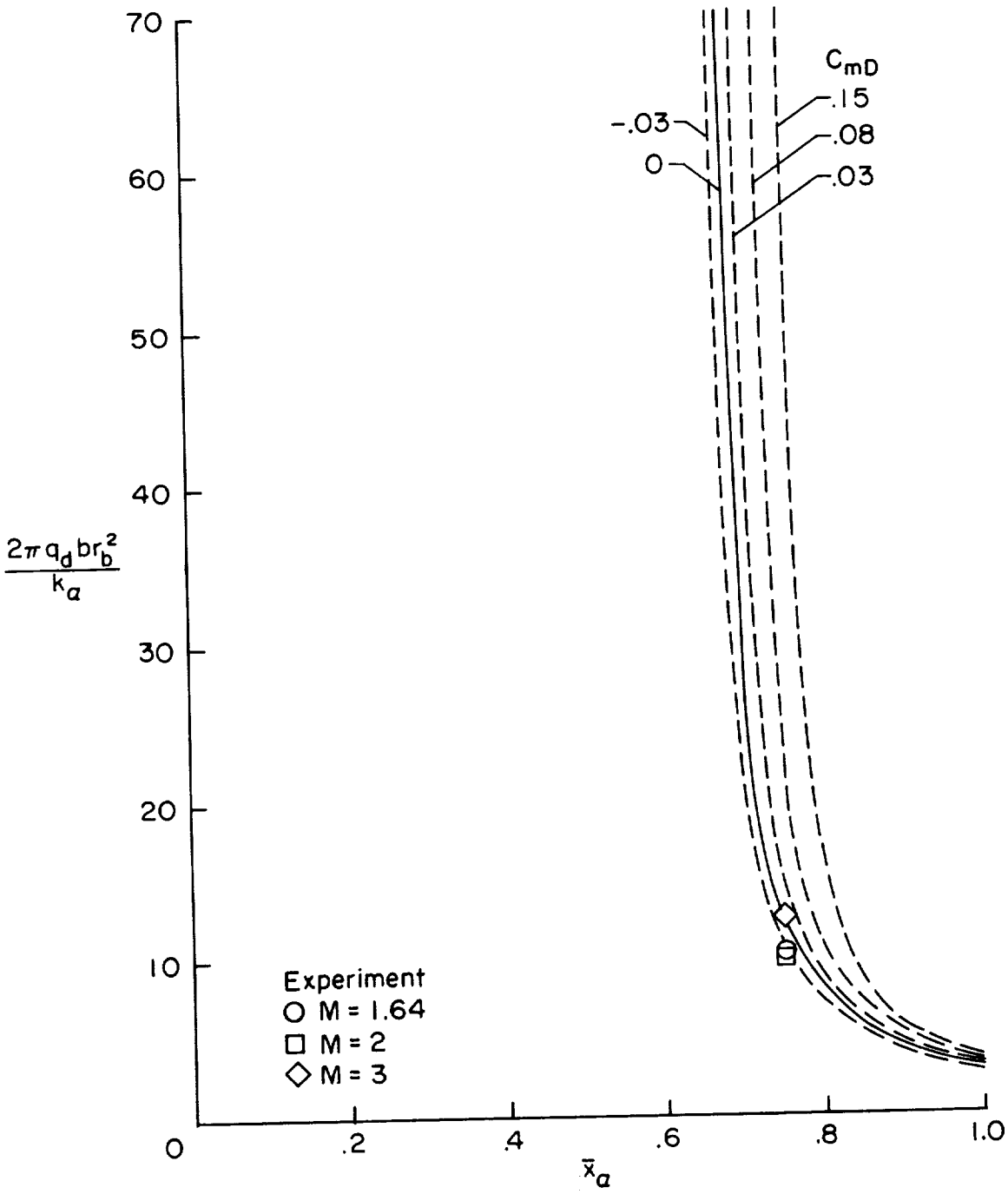

Figure 21.- Effect of steady axial force on divergence behavior of a spring-mounted cone for Munk-Jones and Newtonian (F/δ = 2) theories.